学位論文

The transcription factor Klf5 is essential for intrahepatic biliary epithelial tissue remodeling against liver injury

（転写因子 Krüppel-like factor 5 による 肝障害時における肝内胆管の適応的リモデリング）

平成２９年１２月　博士（理学）　申請

東京大学大学院理学系研究科

生物科学専攻

岡田甫

Table of Contents

List of Abbreviations

BEC: biliary epithelial cell
DR:ductular reaction
LPC: liver stem/progenitor cell
Klf5: Krüppel-like factor 5
NPC: non-parenchymal cell
DDC: 3,5-diethoxycarbonyl-1,4-dihydrocollidine
WT: wild-type
LKO: liver epithelial specific knockout
ALP: alkaline phosphatase
T-BIL: total bilirubin
ALT: alanine aminotransferase
AST: aspartate aminotransferase
Prom1: promonin-1
3D: three-dimensional
TAA: thioacetamide
rAAV2/8: recombinant human adeno-associated virus 2 vector pseudo-serotyped with type 8 capsid
HKO: hepatocyte specific knockout
Fgf7: fibroblast growth factor 7
TWEAK: tumor necrosis factor-like weak inducer of apoptosis
HGF: hepatocyte growth factor
DEG: differential expression genes
GO: Gene ontology
GSEA: Gene set enrichment analysis
TUNEL: terminal deoxynucleotidyl transferase dUTP nick end labeling
ECM: extracellular matrix
PBS: phosphate-buffered saline

Abstract

Under various conditions of liver injury, the intrahepatic biliary epithelium undergoes dynamic tissue expansion and remodeling, a process known as ductular reaction (DR). Mouse models defective in inducing such a tissue-remodeling process are more susceptible to liver injury, suggesting a crucial role of this process in liver regeneration. However, the molecular mechanisms regulating the biliary epithelial cell (BEC) dynamics in DR remain largely unclear. Here, I demonstrate that the transcription factor Krüppel-like factor 5 (Klf5) is highly enriched in mouse liver BECs and plays a key role for regulation of DR, specifically under cholestatic injury conditions. Although mice lacking Klf5 in both hepatocytes and BECs (Klf5-LKO mice) did not exhibit any apparent phenotype in the hepatobiliary system under normal conditions, they exhibited significant defects in biliary epithelial tissue remodeling upon 3,5-diethoxycarbonyl-1,4-dihydrocollidine-induced cholangitis, concomitantly with exacerbated cholestasis and reduced survival rate. In contrast, mice lacking Klf5 solely in hepatocytes did not exhibit any such phenotypes, confirming Klf5's specific role in BECs. RNA-Seq analyses of BECs isolated from the Klf5-LKO mouse livers revealed that the Klf5 KO primarily affected expression of cell cycle-related genes. Moreover, immunostaining analysis with the proliferation marker Ki67 disclosed that the Klf5-LKO mice had significantly reduced BEC proliferation levels upon injury. These results indicate that Klf5 plays a critical role in DR and biliary epithelial tissue expansion and remodeling by inducing BEC proliferation, thereby contributing to liver

regeneration.

Introduction

The liver is a vital organ for life and plays an array of critical biological functions, including metabolism, detoxification, serum protein production, and bile secretion. Being inherently susceptible to a wide range of chemicals, toxins, and xenobiotics entering from the intestinal tract through the portal venous flow, the liver has tremendous capability to regenerate itself in response to various types of injury. Although hepatocytes, parenchymal cells of the liver, elicit vigorous regenerative activity through proliferation and self-duplication (1, 2), other non-parenchymal cells in the liver also contribute significantly to the regenerative process, such as by inducing fibrogenesis for temporal repair of tissue architecture, evoking and modulating the immune and inflammatory responses, and supporting hepatocyte renewal (Figure 1).

Among liver non-parenchymal cells, biliary epithelial cells (BECs) compose the bile duct, a conduit system that collects bile produced by hepatocytes and excretes it to the intestine. Although the bile duct is a quiescent tissue under normal conditions, it undergoes dynamic tissue remodeling once the liver is injured; the biliary tree structure arborizes and transforms adaptively so that the branches extend toward the sites of parenchymal injury (3) (Figure 2). This remodeling process is called the ductular reaction (DR) and is associated with various liver disorders in human patients, such as viral hepatitis, acute and chronic cholestasis, alcoholic liver disease, and nonalcoholic fatty liver disease (4). Although the DR has been classically assumed to correspond to

the emergence and expansion of liver stem/progenitor cells (LPC) that differentiate into hepatocytes, thereby contributing to renewal of the parenchymal tissue (5, 6), this notion has been challenged in recent years based on the results obtained from *in vivo* genetic lineage-tracing studies in mice (6, 7). Thus, in most, if not all, cases of liver regeneration upon chronic injury in mice, newly formed hepatocytes are derived almost exclusively from pre-existing hepatocytes rather than LPCs or BECs. Nevertheless, mouse models with attenuated or diminished DR generally suffer from more aggravated liver injury, suggesting that DR is a fundamental physiological reaction for the liver to counter toxic attacks.

DR is a rare tubulogenesis that occurs in the adult stage, not in the developmental stage when most tube formation processes occur; hence it is a very interesting model for tubulogenesis to understand the diversity of the tube formation process, in addition to its clinical significance. Tubulogenesis is a fundamental and coordinated process for multicellular organisms to achieve transportation of liquids and gas throughout the body. Bile duct formation during embryogenesis definitely undergo following morphogenesis steps; first, precursor cells of BECs form a continuous single-layered ring (ductal plate) around the portal mesenchyme; second, the ductal plate becomes partially bilayered; third, focal dilations appear between the two cell layers, giving rise to the bile ducts (8). In contrast to such a pre-determined morphogenesis step during bile duct development regulated by the built-in signals, DR is the adaptive transformation process that changes the biliary structure into various tube morphologies against the injury; hence there

plausibly supposed to be diverse molecular mechanism regulating DR to achieve the various morphologies of bile duct against the various injury. As DR is induced by coordinated actions of BECs and other liver cell types, several kinds of humoral factors and extracellular signals have been identified that regulate proliferation and differentiation of BECs (9–11). In contrast, it still remains largely unknown how BEC intrinsic genetic programs and gene regulatory networks that regulate DR. Previous identified outside signals are certainly important; however, they seem to act on BECs not solely but simultaneously and have functional redundancy (e.g. BECs proliferation) in the injury conditions so that I thought it is difficult to understand comprehensive molecular gene regulatory networks that regulate DR by the approach focusing on each outside signal. To understand the tube remodeling process of the biliary architecture and especially its underlying mechanism comprehensively, I focused on the BEC transcription factors because they integrate outside signals on BECs arose from various types of injury and instruct the intrinsic gene regulatory networks to form biliary architecture adequately.

Although tube morphology and the formation process vary in organs, signals and molecules that control tube morphologies are conserved among various organs and also species. Especially, fibroblast growth factors (Fgfs) are known to play critical roles in branching morphogenesis to induce proliferation of the tubes and budding branches in many organs and species (12). Because Fgf7 is a member of FGF family and was shown to induce DR as an aforementioned humoral factor in the author's laboratory (11), I

focused on the Fgf7 downstream signal. To identify the BEC intrinsic transcription factor regulating DR, I reanalyzed the microarray data of BECs transcriptional profile presented by Dorrell *et al*. (13) and found fourteen candidate DR regulating transcription factors which are enriched in BEC under the cholestatic injury (data not shown). To further narrow the candidates, I focused *Fgfbp1* which is the Fgf7 downstream target (14) and reported to express in BECs under the cholestatic injury condition (11); and I picked Krüppel-like factor 5 (Klf5) because Klf5 regulates *Fgfbp1* transcriptionally (15) so that I speculated that this transcription factor potentially regulates Fgf7 downstream signal.

Klf5 is a member of Krüppel-like factors, which are versatile transcription factors that play diverse roles in processes such as cell proliferation, differentiation, development and regeneration in a wide range of tissues and cell types (16). Notably, Klf5 has been shown to be involved in the development and maintenance of several kinds of epithelial tissues and organs, including the intestine, lung, and renal collecting duct (17–19). In the small intestine, for example, Klf5 is locally expressed in the crypt and maintains tissue morphology by contributing to the maintenance of intestinal stem cells (20). With regard to the liver, however, there are few reports addressing the role of Klf5 in organ homeostasis and regeneration, although its involvement in hepatocarcinogenesis has been well documented (21). In this study, I revealed that in the mouse liver, Klf5 is a transcription factor that was highly expressed in BECs. *In vivo* studies employing liver cell type-specific knockout mouse models, in combination with multiple liver injury

protocols with different etiologies, delineated a hitherto unidentified role of Klf5 in the biliary epithelium under cholestatic injury conditions.

Materials and Methods

Animals and Liver Injury Models

Wild-type (WT) C57BL/6J mice were purchased from CLEA Japan, Inc. To generate liver epithelial-specific Klf5 KO (Klf5-LKO) mice, mice harboring floxed alleles of the Klf5 gene ($Klf5^{flox/flox}$) (22) were crossed with Alfp-Cre Tg mice (kindly provided by Dr. Klaus Kaestner, University of Pennsylvania) (23). For the hepatocyte-specific Klf5 KO (Klf5-HKO) experiments, the recombinant adeno-associated virus expressing a codon-optimized Cre variant (iCre) under the control of a hepatocyte-specific promoter (rAAV2/8-iCre) (7) was packaged in HEK293 cells according to the protocol described previously (24). iCre was acquired from the pDIRE plasmid, which was a gift from Rolf Zeller [Addgene plasmid # 26745, (25)]. The titered virus was delivered by intraperitoneal injection at a dose of 1×10^{11} vector genomes/mouse.

For injury models, mice were fed a 0.1% DDC-containing diet (F-4643; Bio-Serv) for the DDC model or administered TAA (204-00881; Wako; 300 mg/L) in drinking water for the TAA model. The duration of each injury protocol is indicated in the figure legends. For *in vivo* EdU labeling assays to monitor BEC proliferation, EdU was injected intraperitoneally at a dose of 2 mg/mouse. Overexpression of Fgf7 and Tweak in the mouse liver was achieved by hydrodynamic tail vein injection essentially as described previously (3), with 10 μg of plasmids per 20 g body weight being injected to mice at the age of 6- to 8-week-old.

All animals were maintained under standard specific pathogen-free conditions. All animal experiments were conducted in accordance with the Guideline for the Care and Use of Laboratory Animals of The University of Tokyo, under the approval of the Institutional Animal Care and Use Committee of Institute of Molecular and Cellular Biosciences, The University of Tokyo (approval numbers 2501, 2501-1, 2609, 2706, 2804 and 2904).

Immunostaining analyses with tissue sections

Dissected livers were directly embedded in Tissue-Tek O.C.T. Compound (4583; Sakura Finetek USA, Inc.), and snap frozen. Frozen sections (8 μm) of the liver were prepared using a HM525 cryostat (Microm International) and placed on aminopropyltriethoxysilane-coated glass slides (Matsunami Glass). Fixation was performed with acetone or/and 4% paraformaldehyde after sectioning. After blocking in 3% bovine serum albumin in phosphate-buffered saline (PBS) containing 0.1% Triton X-100 or 3% fetal bovine serum in PBS containing 0.1% Triton X-100, the samples were incubated with primary antibodies described in Table 3 and then with fluorescence-conjugated secondary antibodies. Nuclei were counterstained with Hoechst 33342 (Sigma). Liver sections were imaged with fluorescence microscopes (Axio Observer.Z1, Zeiss; IX83, Olympus) and a confocal laser-scanning microscope (Fluoview FV1200 and FV3000, Olympus). Immunostaining of 200-μm tissue sections was performed according to the protocol described previously (3). For 3D presentation,

surfaces were virtually constructed using the “Surface” function in IMARIS software (Bitplane).

TUNEL assay was performed using the In Situ Apoptosis Detection kit (MK500; TaKaRa) according to the manufacturer’s instructions, and the fluorescence signal was enhanced by treating the samples with AlexaFluor488-conjugated anti-fluorescein antibodies (200-542-037, Jackson ImmunoResearch Laboratories Inc.).

Quantitative analyses in tissue sections

For the quantification of positive areas with CK19 expression (Figure9B, Figure 14B, Figure 15B, and Figure 18C), immunostained whole liver sections were imaged and quantified using an IN Cell Analyzer 2000 (GE Healthcare). The ratio of $CK19^+$ area per total liver area was calculated. More than three mice were used for each of the control and Klf5-LKO groups in all experiments. For BEC proliferation and apoptosis assays in Figure 23 and Figure 25, numbers of $Ki67^+/CK19^+$ and $TUNEL^+/CK19^+$ cells were manually counted and the ratios to the total numbers of $CK19^+$ cells were calculated. More than 10 fields in each section were randomly selected for analysis.

For the quantification of biliary branches in the 3D images (Figure 12), confocal image stacks were recorded with a confocal microscope (FV3000, Olympus) using a 20×/0.75 NA objective lens (UPLSAPO 20X; Olympus). Settings used were: 800 × 800 pixel frame size; 795 nm pixel size; 1.02 μm z-distances between sections; and a 12.5 ms/pixel scan speed. Each visual field was acquired in a uniform size; 636.396 μm × 636.396 μm in the X-Y plane, throughout the full length of the Z-axis to represent the

entire structure in 200-μm-thick tissue sections. For 3D images, Gaussian smoothing (0.795 voxel radius) was performed. Biliary branches were skeletonized as filaments (as exemplified in Figure 12A) and the length and volume size of each branch segment were quantified using the "Filament Tracer" application attached to IMARIS. When comparing the thickness of biliary branches (Figure 12C), "branch thickness index" was calculated as the square root of the quotient obtained by dividing the branch volume size by the branch length.

Cell preparation and flow cytometry

Preparation of cell fractions from adult mouse livers was performed as described previously (26). Briefly, a single cell suspension from the mouse liver was obtained by a two-step collagenase perfusion method and the parenchymal (hepatocyte) and non-parenchymal cell (NPC) fractions were prepared by centrifugal separation. To prepare the BEC fraction, NPCs were treated with anti-EpCAM monoclonal antibody (Table 3) and the samples were sorted by Moflo XDP (Beckman-Coulter). Non-viable cells were excluded by propidium iodide staining.

In the EdU incorporation experiments, NPCs were co-stained with anti-EpCAM and anti-CD45 antibodies and BEC fractions were identified as an $EpCAM^{+}$ $CD45^{-}$ cell population. EdU detection was performed by using the Click-iT Plus EdU Alexa Fluor 488 Cytometry Assay Kit (Life Technologies), following the manufacturer's instructions. The samples were analyzed by FACSCanto II (BD Biosciences). Non-viable cells were excluded by Fixable Viability Stain 450 (BD Biosciences).

Gene expression analysis by quantitative RT-PCR

Total RNA was isolated from whole liver samples or sorted cell populations using TRIzol reagent (Invitrogen), treated with DNaseI (Invitrogen), and then used for cDNA synthesis with PrimeScript RT Master Mix (Takara). Quantitative RT-PCR analyses were performed using LightCycler (Roche) with SYBR Premix Ex Taq (Takara). *Gapdh* was used as the internal control. Primer sequences are listed in Table 1.

Genomic PCR analysis for* Klf5 *deletion

Isolated hepatocytes, BECs, and NPCs (1.0×10^2 cells for each) were lysed in a buffer containing 65 mM Tris-HCl, pH 8.8, 16.6 mM ammonium sulfate, 1 mM 2-mercaptoethanol, 6.7 μM EDTA, and 0.5% Triton X-100. The lysates were subjected to genomic PCR amplification of the *Klf5* gene locus with Tks Gflex DNA Polymerase (Takara) using Thermal Cycler (Bio-Rad). Primer sequences are listed in Table 2. Cycling conditions were as follows: 98°C for 1 min; followed by 40 cycles of 98°C for 10 sec, 62°C for 15 sec and 68°C for 3 min; and a final, 10 minute elongation step at 68°C. The amplified samples were analyzed by agarose gel electrophoresis along with DNA size markers (100 bp ladder and 1 kb ladder: New England Biolabs).

RNA-Seq

BEC populations were prepared by cell sorting from the control and Klf5-LKO mice treated with DDC for one week (N = 3 mice for each genotype; $1.0\text{-}1.7 \times 10^4$ cells per

sample). The cells obtained from each one mouse was individually used to prepare a RNA-Seq library (resulting in 6 libraries in total). Total RNA was isolated using the TRIzol reagent (Invitrogen), treated with DNaseI (Invitrogen) and purified using TRIzol reagent again. Total RNA samples that met the quality control thresholds (RNA integrity RIN > 8.5) were used to prepare barcoded libraries with the SMARTer Ultra Low Input RNA Kit for Sequencing - v3 (Takara) and subsequently with the Nextera XT DNA Library Preparation Kit (Illumina) according to the manufacturers' instructions. Library samples were sequenced on HiSeq 2000 (Illumina).

RNA-Seq data analysis

The first 14 bases from each read were trimmed, and the subsequent 52 bases were aligned to the *Mus musculus* genome (UCSC mm10) using Tophat. Only the reads that uniquely aligned to the transcripts were counted. Transcript counts were normalized, and differential gene expression was calculated using DESeq2 package in R (27). Significant DEG were selected based on a false-discovery q-value cutoff of 0.1. GO analysis was performed using the DAVID database (28). GSEA was employed to identify significantly affected biological pathways using the GO biological process modules, the KEGG gene sets modules and Reactome gene sets modules. After Kolmogorov–Smirnoff testing, the gene sets showing NOM p-val < 0.05 and FDR q-val < 0.25 were considered enriched. RNA-seq fastq files and processed data files were deposited into the NCBI database under accession number GSE97167.

RNA-Seq fastq files on intestinal crypt samples from the intestine-specific Klf5 KO and control mice (29, 30) were obtained from GEO database under accession number GSE79758 ("Differential gene expression in intestinal mouse crypts after loss of KLF5"). These data were also analyzed as described above.

Statistical Analysis

Data are expressed as the mean ± standard deviation of the mean (SD). The *Shapiro-Wilk* test was used to assess the normality of distribution of investigated parameters, and significant differences were tested using the unpaired two-tailed Mann Whitney *U* test or Student *t* test accordingly. Statistical analyses were performed using the R software and the Prism software (GraphPad, San Diego, CA). Differences were considered statistically significant at $P < 0.05$.

Results

Klf5 is expressed predominantly in biliary epithelial cells in the liver

To identify candidate transcription factors that are expressed in BECs and are potentially involved in regulation of DR, I utilized publicly available BEC transcriptome datasets. A previous study by Dorrell *et al*. (13) examined mRNA profiles of the BEC-enriched non-parenchymal cell fractions ("ductal NPC" fractions) sorted from the liver of both normal and 3,5-diethoxycarbonyl-1,4-dihydrocollidine (DDC)-treated mice based on the expression of surface markers. DDC administration is a well-established model for chronic and cholestatic liver injury in mice, which accompanies typical DR induction. Upon examining the gene expression data profile, with a particular focus on transcription factors, I noticed that expression of *Klf5* was highly enriched in MIC1C3^{+}/CD133^{+}/CD26^{-} BEC fractions, particularly under DDC-induced injury conditions (data not shown). Of note, as Klf5 transcriptionally regulates *Fgfbp1* that is a target of Fgf7 signaling (15, 14), I was motivated to explore the possibility that this transcription factor mediates the Fgf7 signal to DR.

To reveal a potential role of Klf5 in regulating DR in injured livers, I first confirmed its expression profile in the DDC-induced mouse liver injury model. Quantitative reverse transcription-polymerase chain reaction (RT-PCR) analysis using whole liver samples revealed that *Klf5* was expressed in the liver and that its expression level increased significantly in the time course of injury, along with that of the BEC marker

Epcam (Figure 3). To determine whether *Klf5* is expressed in BECs, I isolated BECs using a cell sorter based on the expression of EpCAM as a cell surface antigen of BECs. RT-PCR analysis revealed that *Klf5* expression was highly enriched in the $EpCAM^{+}$ BEC fraction, whereas it was barely detected in other non-parenchymal cells or hepatocytes, both under normal conditions and DDC injury conditions (Figure 4). Of note, the levels of *Klf5* expression in BECs were comparable under the normal and injured conditions. Immunostaining analysis of liver sections also showed that Klf5 was predominantly expressed in BECs in both normal and injured livers (Figure 5).

Liver-specific *Klf5*-knockout mice develop normally with no obvious defect in the liver under normal conditions

To assess the functional involvement of Klf5 in DR regulation *in vivo*, I crossed *Klf5* flox mice (22) with the *Alfp-Cre* transgenic mice (23) to produce liver epithelial cell-specific *Klf5* conditional knockout mice (*Alfp-Cre*$^{Tg/+}$;*Klf5*$^{flox/flox}$). In the *Alfp-Cre* transgenic line, the Cre recombinase is expressed under the control of the α-fetoprotein (*Alfp*) gene enhancer and the albumin (*Alb*) gene promoter and starts to be expressed in fetal liver hepatoblasts, which are bi-potential stem/progenitor cells giving rise to hepatocytes and BECs in the postnatal liver; thus, Cre-mediated recombination at a target locus is initially induced in hepatoblasts and hence is inherited and present in the entire epithelial cell lineages in the adult liver, including hepatocytes and BECs, as well as LPCs upon liver injury (Figure 6A) (11). It should be noted that expression of *Alfp-Cre* in the adult liver, which might possibly be induced more strongly in cells with

stem/progenitor-like characters, does not affect this recombination pattern in principle. In addition, the recombination does not occur in other, non-epithelial lineages, such as sinusoidal endothelial cells or hepatic stellate cells, as they originate from distinct types of lineage-specific progenitor cells other than hepatoblasts and do not express *Alfp* or *Alb*.

Nevertheless, I empirically determined the recombination profile in the compound mutant mice and, as expected, genomic PCR analysis revealed that deletion of Klf5 was achieved efficiently and specifically in both hepatocytes and BECs, but not in other NPCs, in the *Alfp-Cre*$^{Tg/+}$*;Klf5*$^{flox/flox}$ mouse liver (Figure 6B). Immunostaining analysis also confirmed the complete absence of Klf5 protein expression in the liver of these mice (Figure 6C), which are referred to as Klf5-LKO mice hereafter.

Although the systemic deletion of the *Klf5* gene has been reported to result in embryonic lethality (31), Klf5-LKO mice were viable and developed normally. No significant difference was observed between the Klf5-LKO and control mice in terms of body weight, liver weight, liver-to-body weight ratio (Figure 7A), and serum tests for liver injury markers (Figure 7B). Hematoxylin and eosin staining (Figure 7C) and immunostaining for BEC markers (Figure 7D) also revealed no histological abnormality in the liver and bile ducts in the Klf5-LKO mice. These results indicate that although expression of Klf5 is clearly detected in BECs, it is likely dispensable for development and function under physiological conditions of the hepatobiliary system.

Ductular reaction upon cholestatic liver injury is suppressed in Klf5-LKO mice

To test whether any functional requirement of Klf5 could be manifested upon liver injury, I next applied the hepatotoxin DDC-induced injury protocol to Klf5-LKO mice. Upon DDC administration, the Klf5-LKO mice exhibited significantly increased mortality compared to the control mice (Figure 8A). In accordance with this observation, the level of DDC-induced cholestasis was aggravated in Klf5-LKO mice as represented by increased serum cholestatic marker levels, alkaline phosphatase (ALP), and total bilirubin (T-BIL) (Figure 8B), whereas the serum levels of hepatocyte injury markers [alanine aminotransferase (ALT) and aspartate aminotransferase (AST)] were not different between the cohorts (Figure 8C).

In control mice, DDC-induced liver injury caused a massive DR, which is remodeling of bile ducts that can be observed in liver sections as expansion and parenchymal invasion of cells expressing BEC markers such as CK19 (Figure 9A). In Klf5-LKO mouse livers, however, DR was completely suppressed at four weeks after administration of DDC. Quantitative analyses of the level of DR induction along the time course of DDC administration showed that there was a significant difference in DR induction between the Klf5-LKO and control mice at two weeks and thereafter (Figure 9B). Immunostaining analyses employing other BEC markers, EpCAM and promonin-1 (Prom1), also showed essentially the same expression pattern as that of CK19 (Figure

10), confirming that DR was severely suppressed in Klf5-LKO mice upon DDC-induced liver injury.

As DR reflects structural transformation of the biliary tree, I also examined the biliary epithelial tissue morphology at the three-dimensional (3D) level. Immunostaining for CK19 using 200 μm-thick tissue sections and subsequent analysis with confocal microscopy (3) revealed that bile ducts in the Klf5-LKO mouse liver contain fewer number of branches than those in the control liver, while that the length or thickness of the branches was not significantly different between the cohorts (Figure 11, Figure 12). Of note, $CK19^+$ cell clusters that were spatially separated from the biliary tree in the Klf5-LKO liver were observed, implicating disorganization of the biliary structure in the absence of Klf5 function.

To determine whether the role of Klf5 in DR regulation can be more generalized, I next assessed the DR phenotype in the Klf5-LKO liver by applying other types of liver injury protocols. Thioacetamide (TAA) is known to induce local hepatocyte injury around the central vein caused by reactive oxygen species, leading to DR induction in the absence of apparent cholestasis (32). Upon induction of the TAA-induced liver injury for 8 weeks, the Klf5 expression in BECs was confirmed to be present both at the mRNA and protein levels in wild-type (WT) mice (Figure 13, A and B). I administrated TAA to Klf5-LKO and control mice and evaluated the level of DR induction by CK19 immunostaining. Expansion of the $CK19^+$ cells was not affected in the Klf5-LKO liver,

indicating that Klf5 is dispensable for DR upon TAA injury, and hence, is not likely a universal regulator for DR (Figure 14). As a model for cholestatic liver injury alternative to the DDC protocol, I utilized the Abcb4 KO mouse model and crossed it with the Klf5-LKO mouse strain. Abcb4 (also known as Mdr2 in mice, homologous to human MDR3) transports phosphatidylcholine into bile and prevents bile acid toxicity, the genetic mutations of which lead to a chronic and cholestatic disorder called progressive familial intrahepatic cholestasis type 3. Accordingly, Abcb4 KO mice exhibit the cholestatic injury phenotype with DR induction as they develop (33, 34), where the expression of Klf5 in the remodeling biliary epithelium was again confirmed (Figure 13, A and C). In the livers of the Abcb4 KO; Klf5-LKO double KO mice, DR was significantly suppressed when compared to the control liver (Figure 15) and $CK19^{+}$ cell clusters that were spatially separated from the biliary tree were also observed in the double KO mouse liver (Figure 16). Taken together, these results suggest that Klf5 plays an essential role in DR induction specifically upon cholestatic liver injury, thereby contributing to amelioration of cholestasis.

BEC-intrinsic expression of Klf5 is responsible for DR regulation

The results from RT-PCR and immunostaining analyses showed that Klf5 was predominantly expressed in BECs and was barely detected in hepatocytes (Figure 4 and Figure 5), which makes it likely that the aforementioned phenotypes in Klf5-LKO mice are attributable to the loss of Klf5 in BECs. A previous study, however, reported expression and a metabolic function of Klf5 in hepatocytes using primary cultured

mouse hepatocytes (35). To eliminate the possibility that Klf5 in hepatocytes may have caused the DR phenotype in Klf5-LKO mice, I assessed the function of Klf5 particularly in hepatocytes. It has been well-established that recombinant human adeno-associated virus 2 vector pseudo-serotyped with type 8 capsid (rAAV2/8) can specifically and efficiently transduce *in vivo* in mouse hepatocytes, but not BECs. I, thus, applied rAAV2/8 expressing an improved version of the Cre recombinase (iCre) under the control of a hepatocyte-specific promoter (7) to *Klf5* $^{flox/flox}$ mice to achieve hepatocyte-specific deletion of *Klf5* (Figure 17A). Genomic PCR analysis revealed that the deletion was achieved efficiently in hepatocytes, but not in BECs (Figure 17B), and these mice (hereafter referred to as Klf5-HKO mice) were then subjected to the DDC liver injury protocol. Induction of DR upon DDC administration was not at all affected in Klf5-HKO mice (Figure 18, B and C), and the survival rates were indistinguishable between Klf5-HKO mice and the control (Figure 18A). These results strongly suggest that Klf5 expressed in BECs *per se* plays a role in DR regulation in a cell-intrinsic manner.

It has been well-documented that induction and expansion of the DR is controlled by several kinds of humoral factors, such as fibroblast growth factor 7 (Fgf7), tumor necrosis factor-like weak inducer of apoptosis (TWEAK), and hepatocyte growth factor (HGF) (9–11). These growth factors and cytokines are produced by liver non-parenchymal cells such as mesenchymal cells, immune cells, and endothelial cells in the wake of injury and inflammatory responses and can act directly on BECs. In the

livers of DDC-treated Klf5-LKO mice, the expression level of neither *Fgf7, Tweak,* or *Hgf* was significantly affected (Figure 19). This further supports the notion that loss of Klf5 affected DR primarily in a biliary epithelial tissue intrinsic manner, rather than through tissue microenvironment or the niche surrounding BECs.

Klf5 regulates proliferation of BECs upon DDC-induced liver injury

To address the mechanism whereby Klf5 induces and regulates DR, I compared gene expression profiles between wild-type and Klf5-deficient BECs under DDC-induced cholestatic condition. As the DR suppression phenotype and exacerbated cholestasis in Klf5-LKO mice were already evident at two weeks of DDC administration (Figure 8B and Figure 9B), I focused on analyzing samples from one-week injured animals to detect the earliest changes at the initial stage of DR. $EpCAM^+$ cells were sorted from livers of Klf5-LKO mice and control mice after one week of DDC treatment and subjected to RNA-sequencing (RNA-Seq) analysis (N = 3 library samples for each genotype). According to the procedures described in Experimental procedures, I was able to identify 440 differential expression genes (DEG) (27), and DAVID gene ontology (GO) analysis (28) showed that they belonged primarily to categories involved in cell cycle regulation (e.g., cell division and mitotic nuclear division) in the Biological Process category (Figure 20). To further estimate the biological processes that could contribute to DR suppression in Klf5-LKO mice, I performed Gene Set Enrichment Analysis (GSEA) using DEG, which allowed us to compare the DEG to particular gene sets that are pre-made according to previously reported information about genes (36).

The results also indicated that Klf5 regulated cellular processes involved in cell cycle progression (Figure 21).

These results from GO analyses are consistent with the notion that Klf5 is a pro-proliferation factor in many types of epithelial cells, including those in normal and cancer tissues, regulating components of both direct accelerators and breaks in the cell cycle (37, 38). Thus, many cyclins, cyclin-dependent kinases (Cdks), and Cdk inhibitors have been reported to be targets of Klf5 (29, 37, 38). I, therefore, compared the DEG identified herein with the one reported in the GEO database from a study on an intestine-specific deletion of Klf5 (Figure 22A) (29). The RNA-Seq data on BECs showed that expression of some cell cycle-related genes was indeed downregulated upon Klf5 deficiency, whereas the set of the genes affected in BECs were not necessarily consistent with those in the intestine (Figure 22, B and C). Quantitative RT-PCR analysis using isolated BEC fractions confirmed that expression of cyclin genes, *Ccna2*, *Ccnb1*, and *Ccnb2*, was significantly suppressed in Klf5-LKO mice under the DDC-induced injury condition (Figure 22C).

To empirically determine the role of Klf5 as a regulator of BEC proliferation in DR, I immunostained liver sections for the proliferation marker Ki67 and quantitated the level of BEC proliferation upon DDC injury (Figure 23). $Ki67^{+}$ cells among the $CK19^{+}$ BEC population reduced significantly in Klf5-LKO mice, suggesting that suppression of DR upon the loss of Klf5 is, in part, due to reduced proliferation rate of BECs. To further

strengthen this notion, I also performed an *in vivo* 5-ethynyl-2'-deoxyuridine (EdU) incorporation assay (Figure 24A). Flow cytometric analysis of EdU^+ cells in BEC fractions isolated from the livers of DDC-injured animals showed that those BECs that entered the cell cycle and had undergone the S phase were significantly reduced in Klf5-LKO mice (Figure 24B). As Klf5 has also been implicated in cell survival by suppressing apoptosis (29, 38, 39), I also investigated whether DR suppression in Klf5-LKO mice was associated with aberrant induction of apoptosis in BECs. *In situ* terminal deoxynucleotidyl transferase dUTP nick end labeling (TUNEL) staining assays using liver sections revealed that $TUNEL^+$ apoptotic cells among the $CK19^+$ BEC population did not increase significantly in Klf5-LKO mice compared with those in the control mice (Figure 25). In addition, the result of GSEA did not show that Klf5 was involved in apoptosis or cell death (Figure 21, A and B).

Among the known signaling molecules and pathways involved in DR regulation, the roles of Fgf7 and Tweak are quite remarkable, in that simple overexpression of either of these factors alone in the healthy adult mouse liver can sufficiently induce DR through BEC proliferation (3, 9, 11). In order to address a possible role of Klf5 as a downstream effector of these pro-proliferative signals in BECs, I overexpressed each of these humoral factors by hydrodynamic delivery of the gene expression plasmids into the liver of Klf5-LKO mice and assessed the BEC proliferation rates by the EdU incorporation assay (Figure 26A). The rate of EdU^+ BECs did not significantly reduce

in Klf5-LKO mice (Figure 26, B and C), suggesting that these factors can affect BEC proliferation independent of Klf5.

The Notch and Wnt signaling pathways are also known to play important roles in promoting DR and BEC proliferation. However, the RNA-Seq data and subsequent pathway analyses using KEGG pathway gene sets revealed that neither Notch or Wnt signaling was significantly affected in the absence of Klf5 expression (Figure 27A, and Figure 28A). More specifically, although Notch1, Notch2, and Jag1 have been reported to be involved in BEC proliferation (40–42), expression levels of these genes as well as their target genes, *Hes1* and *Hey1*, remained unchanged in Klf5-deficient BECs (Figure 28B). Indeed, none of the genes listed in the "KEGG_NOTCH_SIGNALING_PATHWAY" dataset showed differential expression (data not shown). DEG were not enriched in Wnt signaling pathways either (Figure 28A). These results suggest that Klf5 functions as a more proximal factor controlling cell cycle progression in BECs, rather than by acting upstream of or modulating the activities of these signaling pathways in DR induction.

I also subjected the RNA-Seq data to leading edge analysis (36), which enables us to extract the core genes from particular gene sets, and found that the core genes contributing to the "KEGG_FOCAL_ADHESION" and "KEGG_ECM–RECEPTOR_INTERACTION" pathways were *Lama3* and *Lamb3* (Figure 27B). Quantitative RT-PCR analysis confirmed that expression of these genes in BECs was

certainly reduced in Klf5-LKO mice (Figure 29A). Both of the *Lama3* and *Lamb3* genes encode the components of Laminin-332 (the α3 and β3 subunits, respectively), an extracellular matrix (ECM) protein that is well known to be critically involved in the maintenance of skin architecture by composing hemidesmosome and thereby bridging the epidermis and the underlying dermis (43). Intriguingly, expression of these genes in BECs tended to be augmented specifically under the DDC-induced cholestatic liver injury condition, but not under the TAA-induced injury condition (Figure 29B). This gene expression pattern correlates well with the DR phenotype in Klf5-LKO mice and hence suggests that Laminin-332 may be a critical target molecule of Klf5 to maintain biliary architecture under the cholestatic liver injury conditions.

Discussion

The transcription factor Klf5 has been shown to play diverse roles in various types of tissues and cells, including embryonic stem cells, vascular endothelial cells, fibroblasts, and epithelial cells. *In vivo* studies using several kinds of tissue-specific conditional knockout mice have revealed that Klf5 is critically involved in developmental morphogenesis and/or in maintenance of tissue morphology and functions against injury in multiple epithelial tissues, such as tissues in the intestine, lung, and kidney. Here, I have demonstrated for the first time that Klf5 also plays a physiologically important role in yet another epithelial tissue the intrahepatic biliary epithelium, specifically under cholestatic liver injury conditions. Notably, based on a transcriptomic meta-analysis that compared a large number of microarray data, a very recent report by Passman *et al*. suggested that Klf5 is a candidate marker molecule for LPCs (44). This notion is consistent with the present finding that expression of the gene was highly enriched in BECs in the injured liver, which corresponds to LPCs, among liver cell populations (Figure 4).

DR is a histopathological phenomenon that can be typically recognized by microscopic observation of tissue sections as an ectopic emergence and expansion of biliary-like cells in the parenchymal region upon liver injury. Recent studies have established that it actually represents dynamic remodeling of the tree-like structure of the intrahepatic biliary epithelial tissue. A characteristic feature of this remodeling is

that the structural transformations of the biliary tree are diverse and correlated with the parenchymal injury patterns (3). Thus, under the DDC-induced cholestatic injury condition, when hepatocyte damage occurs across the liver parenchyma, including the peri-portal venous region, biliary branches split intricately around the portal vein and expand randomly to the parenchymal area in all directions. In the TAA model, where zonal metabolizing activity restricts production of toxic metabolites and concomitant hepatocyte injury only to the peri-central venous region, the branches exhibited a different structure that extended in a relatively straight line toward the distant injured area. The present results showed that the involvement of Klf5 was essential for DR induction in the DDC model, but not in the TAA model, strongly suggesting that such a morphological diversity in the biliary remodeling is associated with distinct molecular mechanisms. Hence, this study has further substantiated the concept that DR actually involves phenotypically and mechanistically diverged heterogenic tissue remodeling processes not only at the cellular but also at the molecular level.

The results of quantitative gene expression analysis revealed that expression of the *Klf5* mRNA in BECs was kept constant upon liver injury and under different types of liver injury conditions (Figure 13A). It has been reported that Klf5 proteins undergo several types of post-translational modifications, including acetylation, sumoylation, and phosphorylation, that can modulate their stability, subcellular localization, and/or transactivation activities (45). It is thus possible that the Klf5 function in BECs is

regulated at the post-translational level in a cholestatic liver injury-specific manner, which needs to be addressed in future studies.

The unbiased approach employing the whole transcriptome analysis based on RNA-Seq has shown that Klf5 is primarily involved in regulation of cell proliferation in BECs under the DDC injury condition (Figure 20-22). This was somewhat surprising, as BEC proliferation is induced not only under this particular injury condition but also upon TAA-induced liver injury (7). The previous study has revealed that a select population of BECs proliferates continuously and makes a major contribution in DR induction under the TAA liver injury, although it is not yet defined whether this population is conserved among different types of mouse liver injury models (7). In rat liver injury models, there are different proliferative compartments that differentially respond to the types of liver injury (46–48). Klf5 might regulate cell type-specific proliferation signals in a subpopulation of BECs under cholestatic liver injury.

Studies using various KO mouse models have shown that the Notch, Wnt, Fgf7, and Tweak signaling pathways play important roles in DR induction, particularly under the DDC-induced liver injury condition (42, 49–51). In the present RNA-Seq analysis neither of the Notch or Wnt signaling pathways was significantly affected by the lack of Klf5 expression, nor did the MAP kinase, Akt, or NF-kB pathways, which are the potential downstream signaling mechanisms for Fgf7 or Tweak (Figure 21, Figure 27A, and Figure 28). Hence, Klf5 does not likely function as an upstream regulator and may

rather play a role as a downstream effector and/or a transcriptional coactivator in relation to these pathways. A very recent report suggested that Wnt non-canonical signaling pathway, not the β-catenin-dependent canonical pathway, is involved in DDC induced-BEC proliferation (51). Notably, Klf5 is a biologically relevant target of Wnt1 signaling that is activated in a β-catenin-independent manner in a mammary epithelial cell line (52). This Wnt non-canonical signal, however, upregulates Klf5 at the mRNA level. As the expression level of *Klf5* mRNA in BECs did not increase in the DDC-injured liver compared to that in the normal liver (Figure 4 and Figure 13A), the relevance of the relationship between Wnt1 signaling and Klf5 in DR induction requires further investigation.

With regard to Fgf7 and Tweak, I examined their possible roles as upstream signals for Klf5 more directly by employing *in vivo* gene expression and DR induction experiments in the mouse liver. Contrary to my expectations, the results indicated that Fgf7 and Tweak were capable of inducing BEC proliferation even in the absence of Klf5 (Figure 26, B and C), suggesting that Klf5 is not the primary target of these signals. It should be noteworthy that in those experimental settings DR and BEC proliferation were achieved without any induction of liver injury or concomitant inflammatory responses. A number of studies have pointed out a function for Klf5 as a mediator of external stress responses following tissue injuries, such as those provoked by the bacterial membrane component lipopolysaccharide or ionizing radiation (53, 54). Cholestatic injury conditions cause damages and stresses directly on BECs (55, 56) and

hence could be the trigger for the Klf5 activation. Humoral signals such as Fgf7 and Tweak may act cooperatively with the stress-activated Klf5 and their modes of action on BECs could differ under liver injury conditions.

In organs and tissues containing epithelial cells, Klf5 regulates diverse biological functions. In many cases, the loss of Klf5 affects cell proliferation conspicuously, with several cell-cycle associated genes being identified as critical targets of this transcription factor. *Ccnb1*, *Ccnd1*, *Cdk1*, and *Cdkn2b* have been reported to be direct targets, substantiated by *in vitro* assay, and also in a study using intestine-specific Klf5 KO mice (29, 37, 38, 57–60), whereas the present RNA-Seq showed that only *Ccnb1* and *Cdk1* were significantly affected on loss of Klf5 in BECs (Figure 22). Moreover, Klf5 is involved in the maturation, and not the proliferation, of lung epithelial cells (19). These findings together indicate that Klf5 functions are not necessarily consistent among the different epithelial cell types and that even cell cycle-related genes critically regulated by Klf5 may vary depending on the context of the cell types. It has been reported that Klf5 regulates gene expression in concert with other cell type-specific transcription factors (61, 62), which may render Klf5 with such diverse transcriptional abilities and functions in context-dependent manners.

In Klf5-LKO mice upon DDC administration, the level of DR induction as revealed by $CK19^{+}$ area seemed to increase slightly during the very early phase and peaked around 1-2 weeks after the onset of injury, after which time point it tended to reduce gradually

(Figure 9B). As the proliferation of BECs was still weakly induced, albeit significantly suppressed, in the Klf5-LKO mice (Figure 23 and Figure 24), the observed DR phenotype suggests that Klf5 likely contributes in regulating cellular functions other than proliferation in BECs. Of note, 3D immunostaining analysis showed that some $CK19^+$ cell clusters were certainly separated from the bile ducts upon DDC administration in Klf5-LKO mice (Figure 11), suggesting that Klf5 may be involved in maintaining tissue structural integrity of bile ducts against biliary pressure and/or cholangitis under the cholestatic conditions. Epithelial cells in general, including BECs, are structurally supported by ECMs and receive signals from ECM proteins. It is well established that in the course of bile duct development, ECMs such as α1-containing laminin and α5-containing laminin play fundamental roles by regulating initiation of tubulogenesis and maturation of the duct structure, respectively (63). At the adult stage, remodeling of ECMs such as collagens and laminins occurs along with DR induction when the liver is injured, and functional evidence has been accumulated stating that selective contribution of DR to biliary maintenance or hepatocyte differentiation depends on the types of ECMs, suggesting a close relationship between ECMs and DR regulation (64). Intriguingly, GSEA pathway analysis of the present RNA-Seq data revealed four pathways that were significantly affected by Klf5 deletion, among which "ECM–receptor interaction" and "focal adhesion" were included (Figure 27A). Moreover, I identified the laminin-332 components Lama3 and Lamb3 as candidate Klf5 target genes in BECs (Figure 29). This notion is consistent with a previous study by Shinoda *et al.* showing by microarray analyses that expression of genes related to

ECMs and adhesion molecules, including *Lama3* and *Lamb3*, was up-regulated by overexpression of Klf5 in a chondrogenic cell line (65). Importantly, the expressions of these laminin component genes in BECs were upregulated specifically under the DDC-induced cholestatic injury condition. Thus, it is tempting to speculate that Klf5 regulates certain aspects of interactions between BECs and the ECM microenvironment, plausibly via laminin-332 deposition, that is critical for maintaining the bile duct structure under conditions of biliary stress. Future studies aimed at elucidating the functional relevance and the modes of action of laminin-332 in the BEC–ECM interaction and the remodeling and maintenance of the biliary epithelial structure should lead to further understanding of the molecular mechanisms underlying DR induction under cholestatic liver injury conditions.

Conclusion

DR is a dynamic remodeling of the tree-like structure of the intrahepatic biliary epithelial tissue. A characteristic feature of this remodeling is that the structural transformations of the biliary tree are diverse and correlated with the parenchymal injury patterns. The present study showed that Klf5 is enriched in BECs and regulates DR through cell proliferation regulation and maintenance the remodeling/remodeled biliary structure only under the cholestatic-injury model (Figure30A). This study demonstrates the BEC transcription factor that regulates DR under the cholestatic-injury for the first time and indicates other intrinsic genetic signal networks that regulate DR under other types of injury so that this study strongly suggests that such a morphological diversity in the biliary remodeling arose from the parenchymal injury patterns is associated with distinct BEC-intrinsic molecular mechanisms.

I identified Klf5 as a regulator of BEC proliferation and several cyclins as candidate target molecules functioning downstream of Klf5 in DR under cholestatic-injury. Bile ducts in the Klf5-LKO mouse liver contain the fewer number of branches than those in the control liver although the features of branches are normal in the point of length and thickness after DDC-treatment. From the viewpoint of tubulogenesis, this result indicates that there is the mechanism that protects newly remodeling/remodeled biliary branches against the cholestatic-injury in addition to simple cell proliferation. In addition to cell-cycle regulation, Klf5 core function is probably regulation of the BEC–ECM interaction through deposition of laminin-332 by plausibly transcriptional

regulation of *Lama3* and *Lamb3* (Figure30B). Future studies aimed at elucidating the functional relevance and the modes of action of laminin-332 lead to further understanding of the molecular mechanisms underlying DR induction under cholestatic liver injury conditions.

References

1. Michalopoulos, G. K., and DeFrances, M. C. (1997) Liver regeneration. *Science*. **276**, 60–66
2. Michalopoulos, G. K., and Khan, Z. (2015) Liver Stem Cells: Experimental Findings and Implications for Human Liver Disease. *Gastroenterology*. **149**, 876–882
3. Kaneko, K., Kamimoto, K., Miyajima, A., and Itoh, T. (2015) Adaptive remodeling of the biliary architecture underlies liver homeostasis. *Hepatology*. **61**, 2056–2066
4. Gouw, A. S. H., Clouston, A. D., and Theise, N. D. (2011) Ductular reactions in human liver: Diversity at the interface. *Hepatology*. **54**, 1853–1863
5. Duncan, A. W., Dorrell, C., and Grompe, M. (2009) Stem Cells and Liver Regeneration. *Gastroenterology*. **137**, 466–481
6. Miyajima, A., Tanaka, M., and Itoh, T. (2014) Stem/progenitor cells in liver development, homeostasis, regeneration, and reprogramming. *Cell Stem Cell*. **14**, 561–574
7. Kamimoto, K., Kaneko, K., Kok, C. Y.-Y., Okada, H., Miyajima, A., and Itoh, T. (2016) Heterogeneity and stochastic growth regulation of biliary epithelial cells dictate dynamic epithelial tissue remodeling. *Elife*. **5**, e15034
8. Lemaigre, F. P. (2003) Development of the biliary tract. *Mech. Dev.* **120**, 81–87
9. Jakubowski, A., Ambrose, C., Parr, M., Lincecum, J. M., Wang, M. Z., Zheng, T. S., Browning, B., Michaelson, J. S., Baestcher, M., Wang, B., Bissell, D. M., and Burkly, L. C. (2005) TWEAK induces liver progenitor cell proliferation. *J. Clin. Invest.* **115**, 2330–2340
10. Ishikawa, T., Factor, V. M., Marquardt, J. U., Raggi, C., Seo, D., Kitade, M., Conner, E. a., and Thorgeirsson, S. S. (2012) Hepatocyte growth factor/c-met signaling is required for stem-cell-mediated liver regeneration in mice. *Hepatology*. **55**, 1215–1226
11. Takase, H. M., Itoh, T., Ino, S., Wang, T., Koji, T., Akira, S., Takikawa, Y., and Miyajima, A. (2013) FGF7 is a functional niche signal required for stimulation of adult liver progenitor cells that support liver regeneration. *Genes Dev.* **27**, 169–

181

12. Varner, V. D., and Nelson, C. M. (2014) Cellular and physical mechanisms of branching morphogenesis. *Development*. **141**, 2750–2759
13. Dorrell, C., Erker, L., Schug, J., Kopp, J. L., Canaday, P. S., Fox, A. J., Smirnova, O., Duncan, A. W., Finegold, M. J., Sander, M., Kaestner, K. H., and Grompe, M. (2011) Prospective isolation of a bipotential clonogenic liver progenitor cell in adult mice. *Genes Dev.* **25**, 1193–1203
14. Beer, H.-D., Bittner, M., Niklaus, G., Munding, C., Max, N., Goppelt, A., and Werner, S. (2005) The fibroblast growth factor binding protein is a novel interaction partner of FGF-7, FGF-10 and FGF-22 and regulates FGF activity: implications for epithelial repair. *Oncogene*. **24**, 5269–5277
15. Zhi, X., Zhao, D., Zhou, Z., Liu, R., and Chen, C. (2012) YAP promotes breast cell proliferation and survival partially through stabilizing the KLF5 transcription factor. *Am. J. Pathol.* **180**, 2452–61
16. Bialkowska, A. B., Yang, V. W., and Mallipattu, S. K. (2017) Krüppel-like factors in mammalian stem cells and development. *Development*. **144**, 737–754
17. McConnell, B. B., Kim, S. S., Yu, K., Ghaleb, A. M., Takeda, N., Manabe, I., Nusrat, A., Nagai, R., and Yang, V. W. (2011) Krüppel-Like Factor 5 Is Important for Maintenance of Crypt Architecture and Barrier Function in Mouse Intestine. *Gastroenterology*. **141**, 1302–1313
18. Fujiu, K., Manabe, I., and Nagai, R. (2011) Renal collecting duct epithelial cells regulate inflammation in tubulointerstitial damage in mice. *J. Clin. Investig.* **121**, 3425–3441
19. Wan, H., Luo, F., Wert, S. E., Zhang, L., Xu, Y., Ikegami, M., Maeda, Y., Bell, S. M., and Whitsett, J. (2008) Kruppel-like factor 5 is required for perinatal lung morphogenesis and function. *Development*. **135**, 2563–2572
20. Nakaya, T., Ogawa, S., Manabe, I., Tanaka, M., Sanada, M., Sato, T., Taketo, M. M., Nakao, K., Clevers, H., Fukayama, M., Kuroda, M., and Nagai, R. (2014) KLF5 Regulates the Integrity and Oncogenicity of Intestinal Stem Cells. *Cancer Res.* **74**, 2882–2891
21. Maehara, O., Sato, F., Natsuizaka, M., Asano, A., Kubota, Y., Itoh, J., Tsunematsu, S., Terashita, K., Tsukuda, Y., Nakai, M., Sho, T., Suda, G., Morikawa, K., Ogawa, K., Chuma, M., Nakagawa, K., Ohnishi, S., Komatsu, Y.,

Whelan, K. A., Nakagawa, H., Takeda, H., and Sakamoto, N. (2015) A pivotal role of Kruppel-like factor 5 in regulation of cancer stem-like cells in hepatocellular carcinoma. *Cancer Biol. Ther.* **16**, 1453–1461

22. Azami, T., Waku, T., Matsumoto, K., Jeon, H., Muratani, M., Kawashima, A., Yanagisawa, J., Manabe, I., Nagai, R., Kunath, T., Nakamura, T., Kurimoto, K., Saitou, M., Takahashi, S., and Ema, M. (2017) Klf5 maintains the balance of primitive endoderm versus epiblast specification during mouse embryonic development by suppression of Fgf4. *Development*. **144**, 3706–3718
23. Zhang, L., Rubins, N. E., Ahima, R. S., Greenbaum, L. E., and Kaestner, K. H. (2005) Foxa2 integrates the transcriptional response of the hepatocyte to fasting. *Cell Metab.* **2**, 141–148
24. Kok, C. Y., Cunningham, S. C., Carpenter, K. H., Dane, A. P., Siew, S. M., Logan, G. J., Kuchel, P. W., and Alexander, I. E. (2013) Adeno-associated Virus-mediated Rescue of Neonatal Lethality in Argininosuccinate Synthetase-deficient Mice. *Mol. Ther.* **21**, 1823–1831
25. Osterwalder, M., Galli, A., Rosen, B., Skarnes, W. C., Zeller, R., and Lopez-Rios, J. (2010) Dual RMCE for efficient re-engineering of mouse mutant alleles. *Nat. Methods*. **7**, 893–895
26. Okabe, M., Tsukahara, Y., Tanaka, M., Suzuki, K., Saito, S., Kamiya, Y., Tsujimura, T., Nakamura, K., and Miyajima, A. (2009) Potential hepatic stem cells reside in EpCAM+ cells of normal and injured mouse liver. *Development*. **136**, 1951–1960
27. Love, M. I., Huber, W., and Anders, S. (2014) Moderated estimation of fold change and dispersion for RNA-seq data with DESeq2. *Genome Biol.* **15**, 10.1186/s13059-014-0550-8
28. Huang, D. W., Sherman, B. T., and Lempicki, R. A. (2008) Systematic and integrative analysis of large gene lists using DAVID bioinformatics resources. *Nat. Protoc.* **4**, 44–57
29. Bell, K. N. (2016) The Role of Krüpple-like Factor 5 in Normal Intestinal Homeostasis. *Ph.D. thesis*
30. El Marjou, F., Janssen, K.-P., Hung-Junn Chang, B., Li, M., Hindie, V., Chan, L., Louvard, D., Chambon, P., Metzger, D., and Robine, S. (2004) Tissue-specific and inducible Cre-mediated recombination in the gut epithelium. *genesis*. **39**,

186–193

31. Ema, M., Mori, D., Niwa, H., Hasegawa, Y., Yamanaka, Y., Hitoshi, S., Mimura, J., Kawabe, Y., Hosoya, T., Morita, M., Shimosato, D., Uchida, K., Suzuki, N., Yanagisawa, J., Sogawa, K., Rossant, J., Yamamoto, M., Takahashi, S., and Fujii-Kuriyama, Y. (2008) Krüppel-like factor 5 Is Essential for Blastocyst Development and the Normal Self-Renewal of Mouse ESCs. *Cell Stem Cell*. **3**, 555–567
32. Yeh, C. N., Maitra, A., Lee, K. F., Jan, Y. Y., and Chen, M. F. (2004) Thioaceatamide-induced intestinal-type cholangiocarcinoma in rat: An animal model recapitulating the multi-stage progression of human cholangiocarcinoma. *Carcinogenesis*. **25**, 631–636
33. Smit, J. J. M., Schinkel, A. H., Elferink, R. P. J. O., Groen, A. K., Wagenaar, E., van Deemter, L., Mol, C. A. A. M., Ottenhoff, R., van der Lugt, N. M. T., van Roon, M. A., van der Valk, M. A., Offerhaus, G. J. A., Berns, A. J. M., and Borst, P. (1993) Homozygous disruption of the murine MDR2 P-glycoprotein gene leads to a complete absence of phospholipid from bile and to liver disease. *Cell*. **75**, 451–462
34. Mauad, T. H., van Nieuwkerk, C. M., Dingemans, K. P., Smit, J. J., Schinkel, A. H., Notenboom, R. G., van den Bergh Weerman, M. A., Verkruisen, R. P., Groen, A. K., and Oude Elferink, R. P. (1994) Mice with homozygous disruption of the mdr2 P-glycoprotein gene. A novel animal model for studies of nonsuppurative inflammatory cholangitis and hepatocarcinogenesis. *Am. J. Pathol.* **145**, 1237–1245
35. Kumadaki, S., Karasawa, T., Matsuzaka, T., Ema, M., Nakagawa, Y., Nakakuki, M., Saito, R., Yahagi, N., Iwasaki, H., Sone, H., Takekoshi, K., Yatoh, S., Kobayashi, K., Takahashi, A., Suzuki, H., Takahashi, S., Yamada, N., and Shimano, H. (2011) Inhibition of Ubiquitin Ligase F-box and WD Repeat Domain-containing 7α (Fbw7α) Causes Hepatosteatosis through Krüppel-like Factor 5 (KLF5)/Peroxisome Proliferator-activated Receptor γ2 (PPARγ2) Pathway but Not SREBP-1c Protein in Mice. *J. Biol. Chem.* **286**, 40835–40846
36. Subramanian, A., Tamayo, P., Mootha, V. K., Mukherjee, S., Ebert, B. L., Gillette, M. A., Paulovich, A., Pomeroy, S. L., Golub, T. R., Lander, E. S., and Mesirov, J. P. (2005) Gene set enrichment analysis: A knowledge-based

approach for interpreting genome-wide expression profiles. *Proc. Natl. Acad. Sci.* **102**, 15545–15550

37. Tetreault, M.-P., Yang, Y., and Katz, J. P. (2013) Krüppel-like factors in cancer. *Nat. Rev. Cancer*. **13**, 701–713
38. McConnell, B. B., Ghaleb, A. M., Nandan, M. O., and Yang, V. W. (2007) The diverse functions of Krüppel-like factors 4 and 5 in epithelial biology and pathobiology. *BioEssays*. **29**, 549–557
39. Liu, R., Zheng, H.-Q., Zhou, Z., Dong, J.-T., and Chen, C. (2009) KLF5 Promotes Breast Cell Survival Partially through Fibroblast Growth Factor-binding Protein 1-pERK-mediated Dual Specificity MKP-1 Protein Phosphorylation and Stabilization. *J. Biol. Chem.* **284**, 16791–16798
40. Geisler, F., Nagl, F., Mazur, P. K., Lee, M., Zimber-Strobl, U., Strobl, L. J., Radtke, F., Schmid, R. M., and Siveke, J. T. (2008) Liver-specific inactivation of Notch2, but not Notch1, compromises intrahepatic bile duct development in mice. *Hepatology*. **48**, 607–616
41. Zong, Y., Panikkar, A., Xu, J., Antoniou, A., Raynaud, P., Lemaigre, F., and Stanger, B. Z. (2009) Notch signaling controls liver development by regulating biliary differentiation. *Development*. **136**, 1727–1739
42. Fiorotto, R., Raizner, A., Morell, C. M., Torsello, B., Scirpo, R., Fabris, L., Spirli, C., and Strazzabosco, M. (2013) Notch signaling regulates tubular morphogenesis during repair from biliary damage in mice. *J. Hepatol.* **59**, 124–130
43. Kiritsi, D., Has, C., and Bruckner-Tuderman, L. (2013) Laminin 332 in junctional epidermolysis bullosa. *Cell Adh. Migr.* **7**, 135–141
44. Passman, A. M., Low, J., London, R., Tirnitz-Parker, J. E. E., Miyajima, A., Tanaka, M., Strick-Marchand, H., Darlington, G. J., Finch-Edmondson, M., Ochsner, S., Zhu, C., Whelan, J., Callus, B. A., and Yeoh, G. C. T. (2016) A Transcriptomic Signature of Mouse Liver Progenitor Cells. *Stem Cells Int.* **2016**, 10.1155/2016/5702873
45. Dong, J.-T., and Chen, C. (2009) Essential role of KLF5 transcription factor in cell proliferation and differentiation and its implications for human diseases. *Cell. Mol. Life Sci.* **66**, 2691–2706
46. Alpini, G., Glaser, S. S., Ueno, Y., Pham, L., Podila, P. V, Caligiuri, A., LeSage,

G., and LaRusso, N. F. (1998) Heterogeneity of the proliferative capacity of rat cholangiocytes after bile duct ligation. *Am. J. Physiol.* **274**, G767-75

47. LeSage, G. D., Benedetti, A., Glaser, S., Marucci, L., Tretjak, Z., Caligiuri, A., Rodgers, R., Phinizy, J. L., Baiocchi, L., Francis, H., Lasater, J., Ugili, L., and Alpini, G. (1999) Acute carbon tetrachloride feeding selectively damages large, but not small, cholangiocytes from normal rat liver. *Hepatology*. **29**, 307–319
48. Baiocchi, L., Kanno, N., Phinizy, J. O. L., and Francis, H. (2001) Regression of cholangiocyte proliferation after cessation of ANIT feeding is coupled with increased apoptosis. *Am J Physiol Gastrointest Liver Physiol*. **281**, G182–G190
49. Lozier, J., McCright, B., and Gridley, T. (2008) Notch Signaling Regulates Bile Duct Morphogenesis in Mice. *PLoS One*. **3**, e1851
50. Apte, U., Thompson, M. D., Cui, S., Liu, B., Cieply, B., and Monga, S. P. S. (2007) Wnt/β-catenin signaling mediates oval cell response in rodents. *Hepatology*. **47**, 288–295
51. Okabe, H., Yang, J., Sylakowski, K., Yovchev, M., Miyagawa, Y., Nagarajan, S., Chikina, M., Thompson, M., Oertel, M., Baba, H., Monga, S. P., and Nejak-Bowen, K. N. (2016) Wnt signaling regulates hepatobiliary repair following cholestatic liver injury in mice. *Hepatology*. **64**, 1652–1666
52. Taneyhill, L., and Pennica, D. (2004) Identification of Wnt responsive genes using a murine mammary epithelial cell line model system. *BMC Dev. Biol.* **4**, 10.1186/1471-213X-4-6
53. Chanchevalap, S., Nandan, M. O., McConnell, B. B., Charrier, L., Merlin, D., Katz, J. P., and Yang, V. W. (2006) Krüppel-like factor 5 is an important mediator for lipopolysaccharide-induced proinflammatory response in intestinal epithelial cells. *Nucleic Acids Res.* **34**, 1216–1223
54. Li, M., Gu, Y., Ma, Y.-C., Shang, Z.-F., Wang, C., Liu, F.-J., Cao, J.-P., Wan, H.-J., and Zhang, X.-G. (2015) Krüppel-Like Factor 5 Promotes Epithelial Proliferation and DNA Damage Repair in the Intestine of Irradiated Mice. *Int. J. Biol. Sci.* **11**, 1458–1468
55. Fickert, P., Stöger, U., Fuchsbichler, A., Moustafa, T., Marschall, H.-U., Weiglein, A. H., Tsybrovskyy, O., Jaeschke, H., Zatloukal, K., Denk, H., and Trauner, M. (2007) A New Xenobiotic-Induced Mouse Model of Sclerosing Cholangitis and Biliary Fibrosis. *Am. J. Pathol.* **171**, 525–536

56. Trauner, M., Fickert, P., and Wagner, M. (2007) MDR3 (ABCB4) defects: A paradigm for the genetics of adult cholestatic syndromes. *Semin. Liver Dis.* **27**, 77–98

57. Nandan, M. O., Chanchevalap, S., Dalton, W. B., and Yang, V. W. (2005) Krüppel-like factor 5 promotes mitosis by activating the cyclin B1/Cdc2 complex during oncogenic Ras-mediated transformation. *FEBS Lett.* **579**, 4757–4762

58. Guo, P., Zhao, K.-W., Dong, X.-Y., Sun, X., and Dong, J.-T. (2009) Acetylation of KLF5 Alters the Assembly of p15 Transcription Factors in Transforming Growth Factor-β-mediated Induction in Epithelial Cells. *J. Biol. Chem.* **284**, 18184–18193

59. Nandan, M. O., Yoon, H. S., Zhao, W., Ouko, L. a, Chanchevalap, S., and Yang, V. W. (2004) Krüppel-like factor 5 mediates the transforming activity of oncogenic H-Ras. *Oncogene*. **23**, 3404–3413

60. Nandan, M. O., Ghaleb, A. M., Liu, Y., Bialkowska, A. B., McConnell, B. B., Shroyer, K. R., Robine, S., and Yang, V. W. (2014) Inducible intestine-specific deletion of Krüppel-like factor 5 is characterized by a regenerative response in adult mouse colon. *Dev. Biol.* **387**, 191–202

61. Aizawa, K., Suzuki, T., Kada, N., Ishihara, A., Kawai-Kowase, K., Matsumura, T., Sasaki, K., Munemasa, Y., Manabe, I., Kurabayashi, M., Collins, T., and Nagai, R. (2004) Regulation of Platelet-derived Growth Factor-A Chain by Krüppel-like Factor 5. *J. Biol. Chem.* **279**, 70–76

62. Hayashi, S., Manabe, I., Suzuki, Y., Relaix, F., and Oishi, Y. (2016) Klf5 regulates muscle differentiation by directly targeting muscle-specific genes in cooperation with MyoD in mice. *Elife*. **5**, e17462

63. Tanimizu, N., Kikkawa, Y., Mitaka, T., and Miyajima, A. (2012) α1- and α5-containing Laminins Regulate the Development of Bile Ducts via β1 Integrin Signals. *J. Biol. Chem.* **287**, 28586–28597

64. Williams, M. J., Clouston, A. D., and Forbes, S. J. (2014) Links between hepatic fibrosis, ductular reaction, and progenitor cell expansion. *Gastroenterology*. **146**, 349–356

65. Shinoda, Y., Ogata, N., Higashikawa, A., Manabe, I., Shindo, T., Yamada, T., Kugimiya, F., Ikeda, T., Kawamura, N., Kawasaki, Y., Tsushima, K., Takeda, N., Nagai, R., Hoshi, K., Nakamura, K., Chung, U., and Kawaguchi, H. (2008)

Krüppel-like Factor 5 Causes Cartilage Degradation through Transactivation of Matrix Metalloproteinase 9. *J. Biol. Chem.* **283**, 24682–24689

66. Tanimizu, N. (2003) Isolation of hepatoblasts based on the expression of Dlk/Pref-1. *J. Cell Sci.* **116**, 1775–1786

67. Oishi, Y., Manabe, I., Tobe, K., Ohsugi, M., Kubota, T., Fujiu, K., Maemura, K., Kubota, N., Kadowaki, T., and Nagai, R. (2008) SUMOylation of Krüppel-like transcription factor 5 acts as a molecular switch in transcriptional programs of lipid metabolism involving PPAR-δ. *Nat. Med.* **14**, 656–666

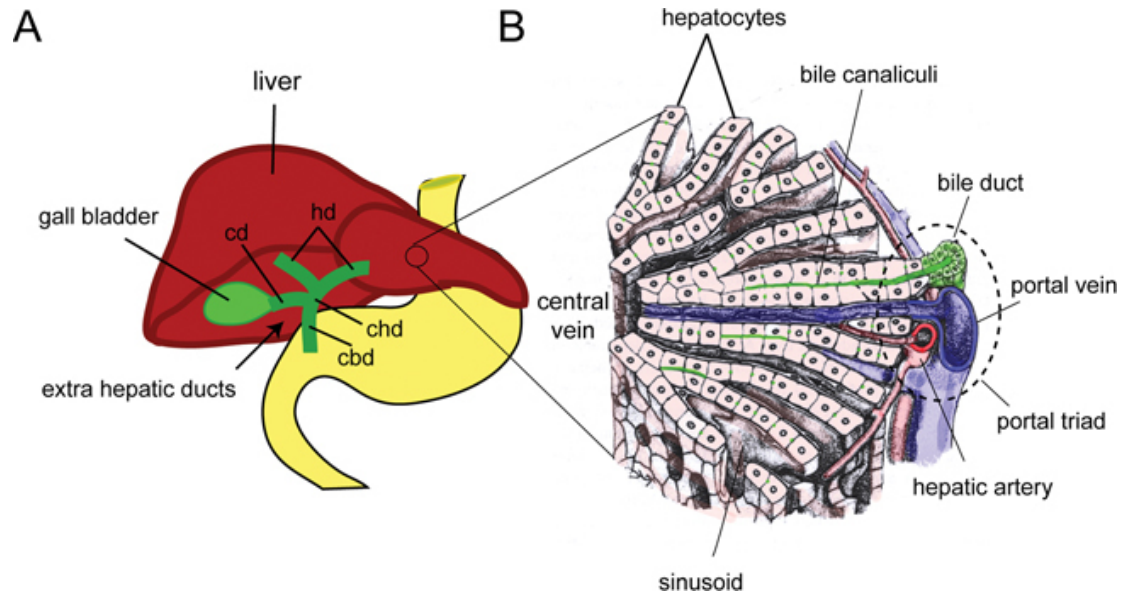

C

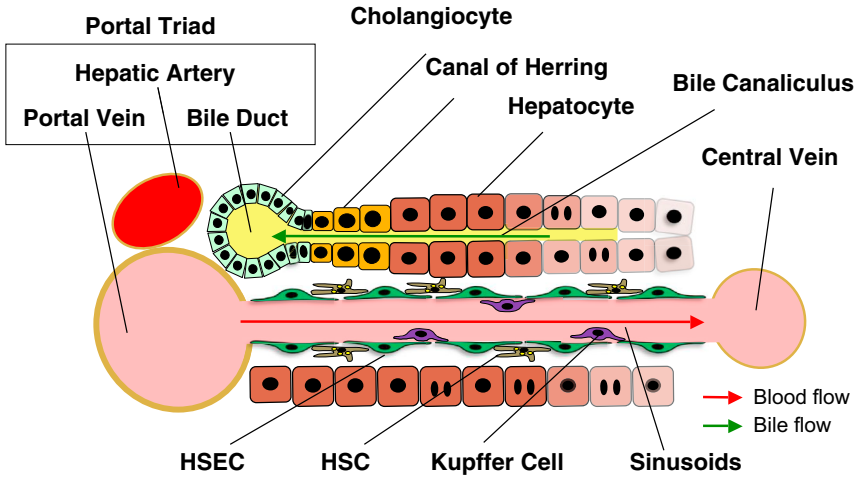

Figure 1. Liver structure

(A and B) These figures show schematic of the liver (from A, Zoan., *StemBook* ("Liver development"), 2008).

(C) This figure shows the structures of sectioned liver tissue (from A. Miyajima et al., *Cell stem cell*, 2014)

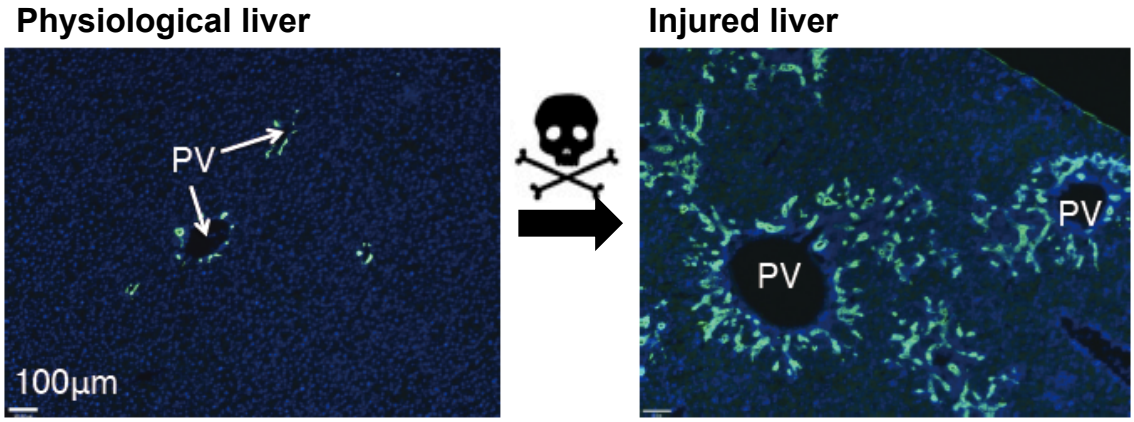

Figure 2. Representative image of ductular reaction

Immunostaining for CK19 (green) in physiological (the left panel) and injured (the right panel) livers shown with counterstaining for nuclei (Blue). PV means Portal Vein.

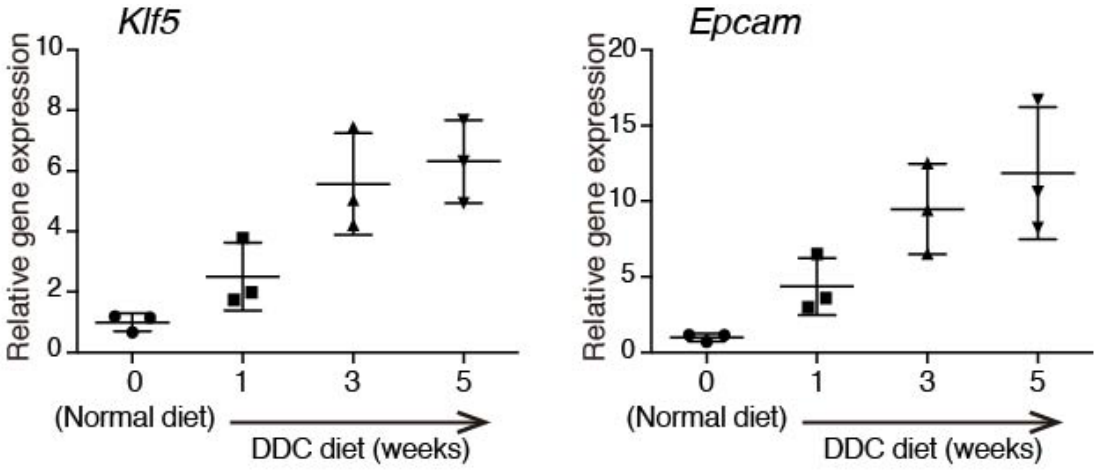

Figure 3. *Klf5* and the BEC marker *Epcam* expression level in the time course of DDC-induced injury

Expression levels of *Klf5* and *Epcam* in whole liver mRNA samples prepared from WT mice were determined by quantitative RT-PCR.

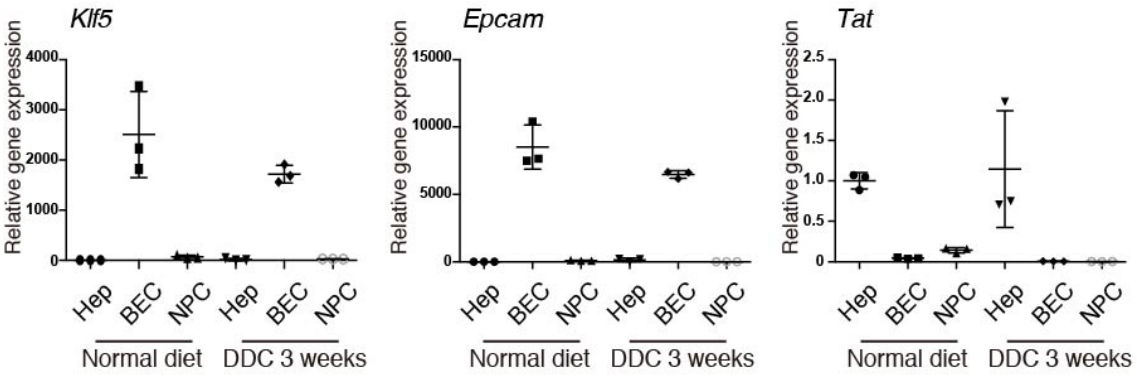

Figure 4. Expression level of *Klf5* in liver cell fractions

Expression level of *Klf5* in liver cell fractions collected from DDC-treated (three weeks) and non-treated (Normal diet) WT mice analyzed by quantitative RT-PCR. Adequate cell fractionations were confirmed by analyses of a BEC marker gene *(Epcam)* and a hepatocyte marker gene *(Tat)*.

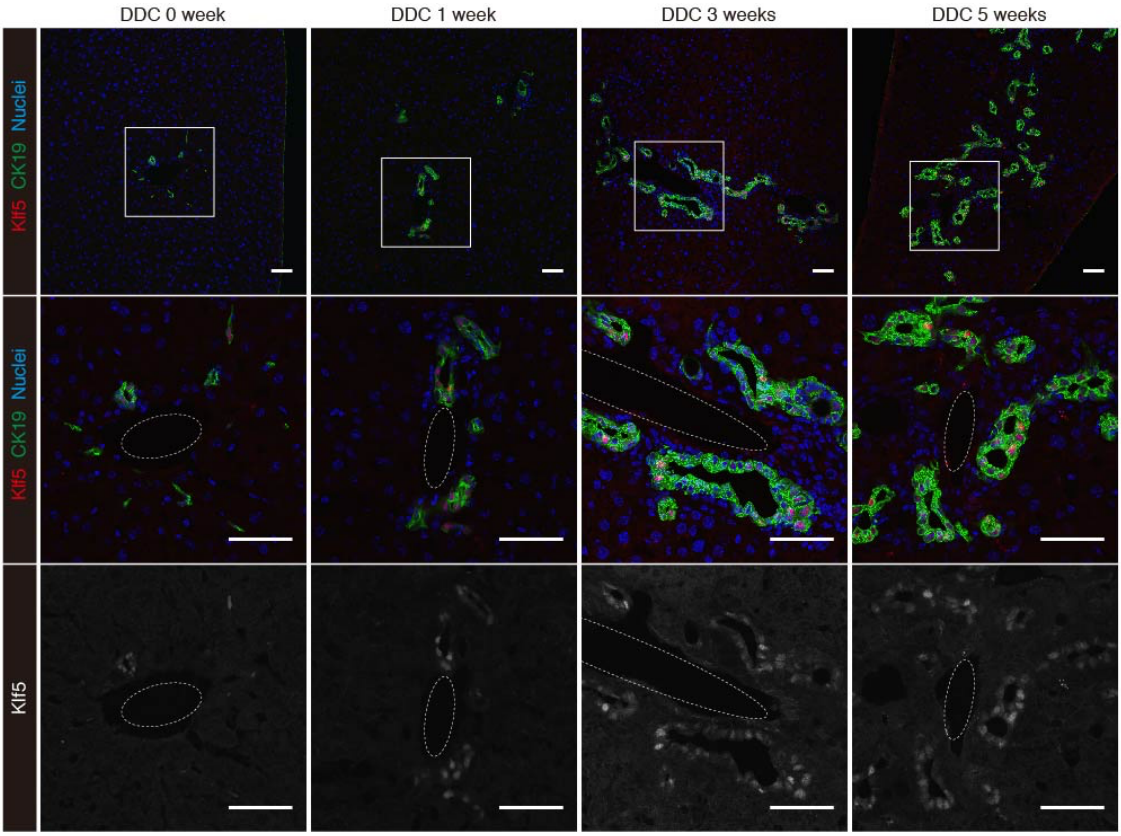

Figure 5. Immunostaining for Klf5 in the time course of DDC-induced injury

Immunostaining for Klf5 (red in the upper and center panels; gray scale in the lower panels) and CK19 (green) in the WT mouse liver. Counterstaining for nuclei is shown in blue (upper and center panels). Regions indicated by white boxes in the upper panels are magnified in the middle and lower panels. Dashed lines show portal veins. Scale bar = 50 μm.

A

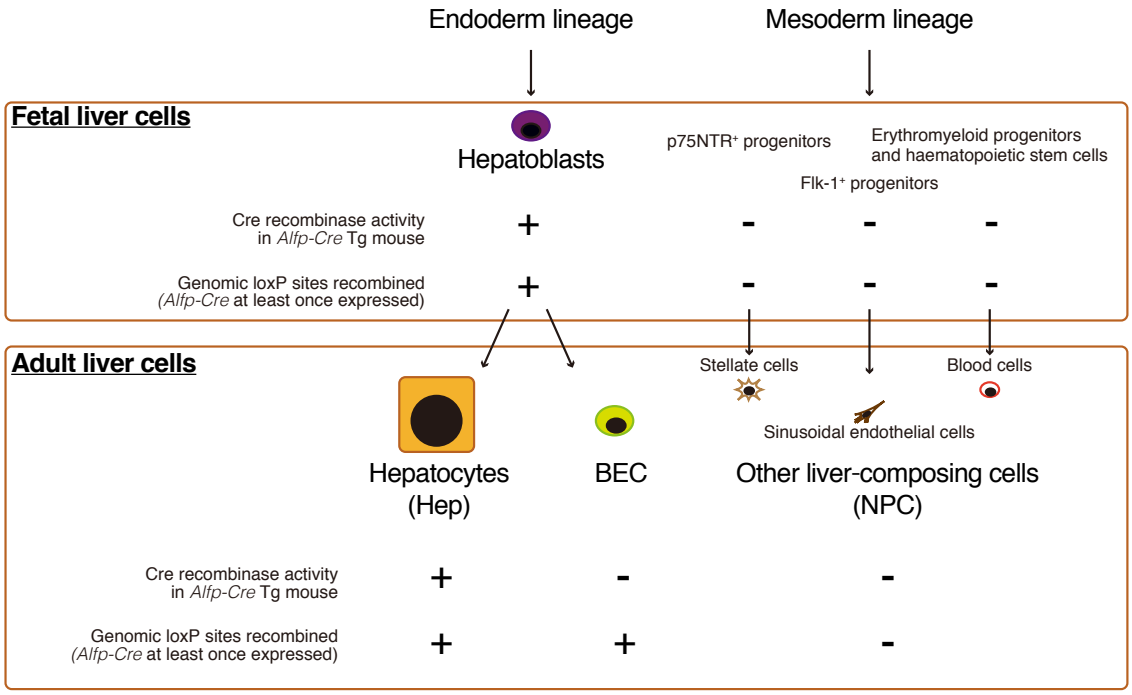
Endoderm lineage
Mesoderm lineage
Fetal liver cells
Hepatoblasts
p75NTR+ progenitors
Erythromyeloid progenitors and haematopoietic stem cells
Flk-1+ progenitors
Cre recombinase activity in Alfp-Cre Tg mouse
Genomic loxP sites recombined (Alfp-Cre at least once expressed)
Adult liver cells
Stellate cells
Blood cells
Sinusoidal endothelial cells
Hepatocytes (Hep)
BEC
Other liver-composing cells (NPC)

B

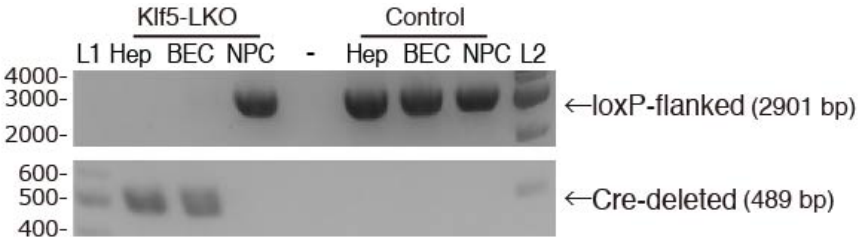
Klf5-LKO
Control
L1 Hep BEC NPC
Hep BEC NPC L2
4000-
3000-
2000-
600-
500-
400-
←loxP-flanked (2901 bp)
←Cre-deleted (489 bp)

C

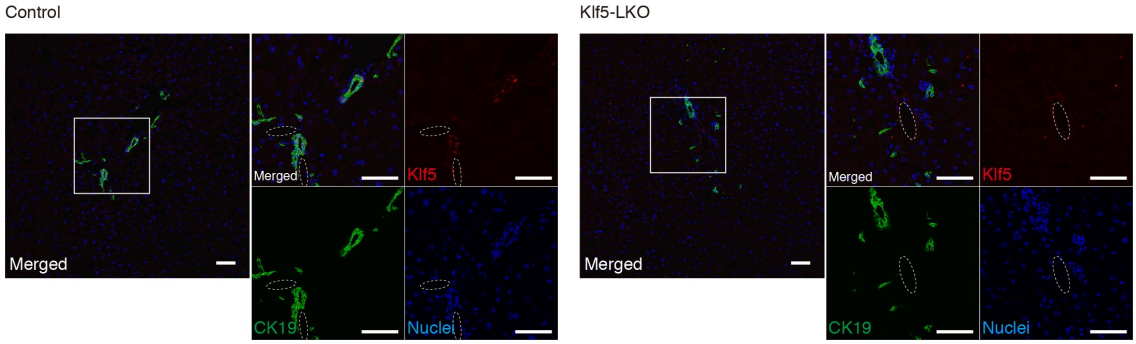
Control
Klf5-LKO
Merged
Klf5
CK19
Nuclei

Figure 6. Liver-specific *Klf5*-knockout mice

(A) Scheme of the course of embryonic liver development and *Alfp-Cre* expression. In the *Alfp-Cre* Tg line, the Cre recombinase under the control of an *Alfp* gene enhancer and an *Alb* gene promoter starts to be expressed in hepatoblasts in the fetal liver, and *Alfp-Cre*–mediated recombination at a target locus is initially induced in hepatoblasts. As *Cre*/*loxP*-mediated genomic recombination is irreversible and inheritable during ontogeny, *Alfp-Cre*–mediated recombination at the target locus should be present in the entire epithelial cell lineages in the adult liver, including hepatocytes and BECs. (B) Genomic PCR analysis for Cre-mediated recombination in the Klf5 locus. The upper and lower panels show amplicons corresponding to non-recombined (floxed) and recombined (Cre-deleted) alleles, respectively. The lanes indicated as L1 and L2 were loaded with 100 bp ladder and 1 kb ladder DNA size markers, respectively. The sizes of markers (bp) are indicated to the left. (C) Loss of Klf5 expression in the Klf5 LKO mouse liver was confirmed at the protein level. Immunostaining results for Klf5 (red) and CK19 (green) are shown with counterstaining for nuclei (Blue). Regions indicated by white boxes in the left panels are magnified in the right panels together with single color channel images. Dashed lines show portal veins. Scale bar = 50 μm.

A

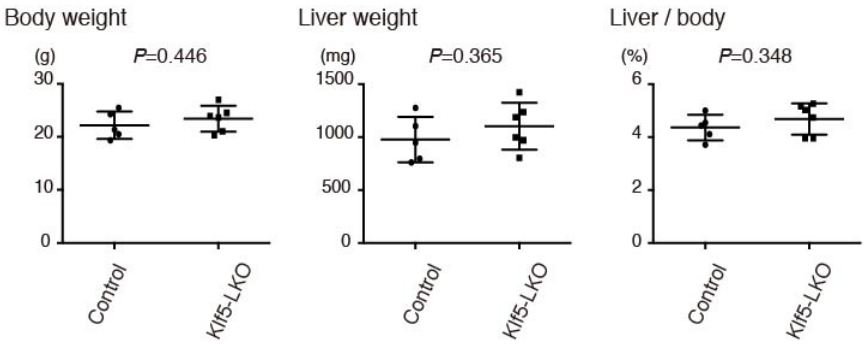
Body weight
(g)
P=0.446
30
20
10
0
Control
Klf5-LKO
Liver weight
(mg)
P=0.365
1500
1000
500
0
Control
Klf5-LKO
Liver / body
(%)
P=0.348
6
4
2
0
Control
Klf5-LKO

B

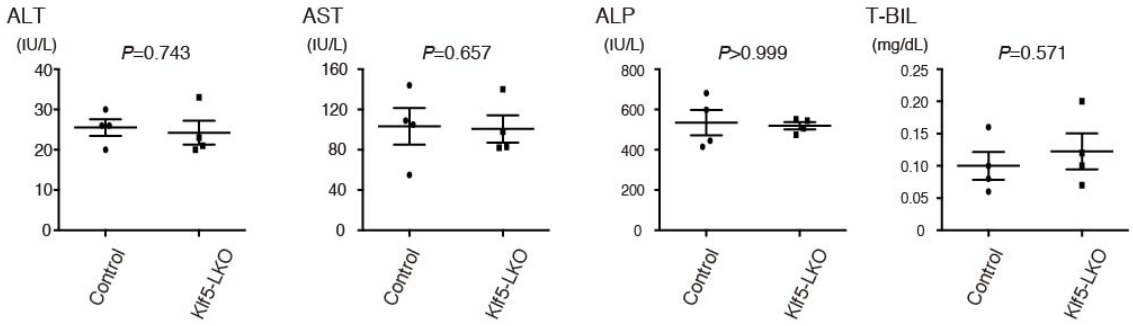
ALT
(IU/L)
P=0.743
40
30
20
10
0
Control
Klf5-LKO
AST
(IU/L)
P=0.657
160
120
80
40
0
Control
Klf5-LKO
ALP
(IU/L)
P>0.999
800
600
400
200
0
Control
Klf5-LKO
T-BIL
(mg/dL)
P=0.571
0.25
0.20
0.15
0.10
0.05
0
Control
Klf5-LKO

C

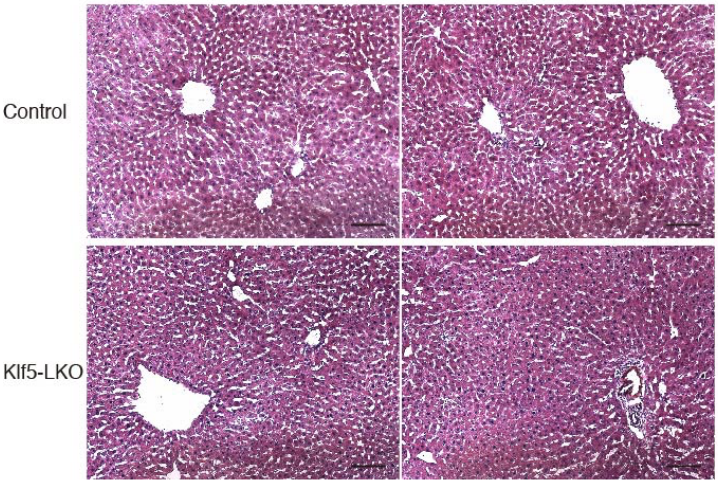
Control
Klf5-LKO

D

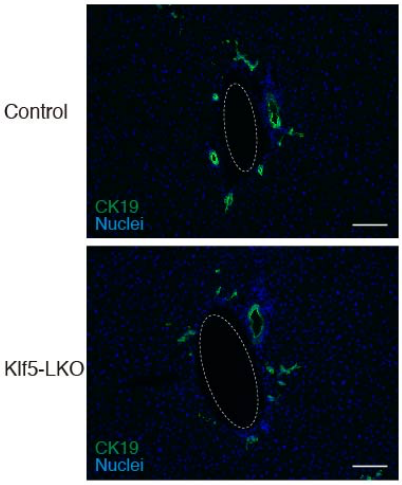
Control
CK19
Nuclei
Klf5-LKO
CK19
Nuclei

Figure 7. Normal liver development in Klf5 LKO mice

(A) Klf5 LKO mice did not show any significant difference from control mice in terms of body weight, liver weight, and the proportion of the liver weight to the body weight. N = 5 and 6 for the control and the Klf5 LKO mice, respectively. P-values calculated by Student *t* test. (B) Serum biochemistry tests for hepatocyte injury markers (ALT and AST) and cholestasis markers (ALP and T-BIL), showing that no liver injury was induced in Klf5 LKO mice under physiological conditions. N = 4 mice for each group. P-values calculated by Mann Whitney *U* test. (C) H&E staining did not show any apparent difference in histology of the liver between the control and Klf5 LKO mice. Scale bar = 100 μm. (D) Immunostaining for CK19 (green) in the Klf5 LKO and control livers in normal conditions. Counterstaining for nuclei is also shown (Blue). Dashed lines show portal veins. Scale bar = 100 μm.

A

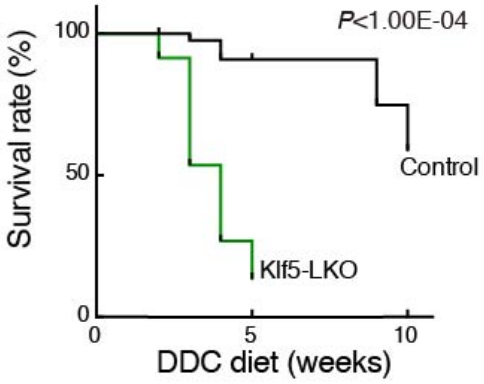
P<1.00E-04
Survival rate (%)
100
50
0
Control
Klf5-LKO
0
5
10
DDC diet (weeks)

B

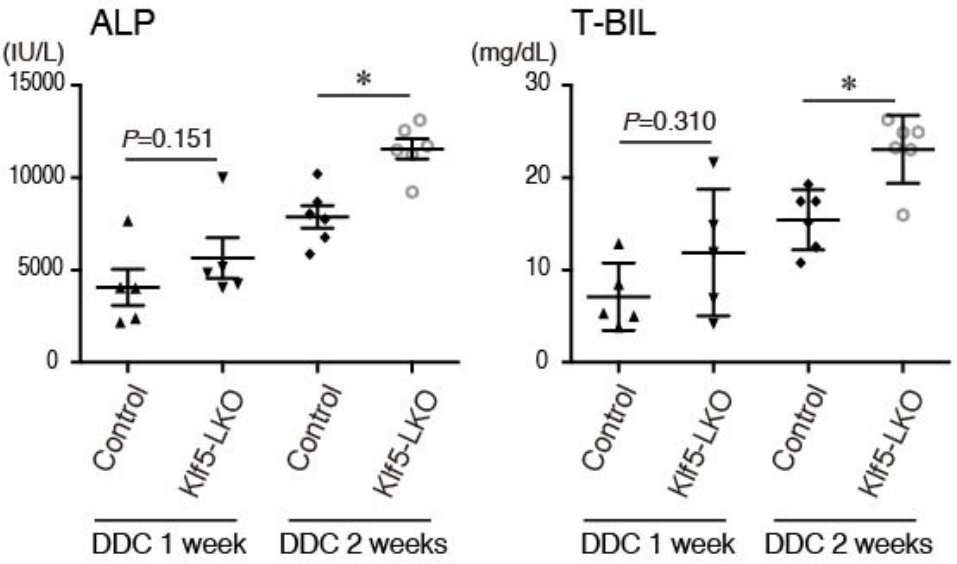
ALP
(IU/L)
15000
10000
5000
0
P=0.151
*
Control
Klf5-LKO
Control
Klf5-LKO
DDC 1 week
DDC 2 weeks
T-BIL
(mg/dL)
30
20
10
0
P=0.310
*
Control
Klf5-LKO
Control
Klf5-LKO
DDC 1 week
DDC 2 weeks

C

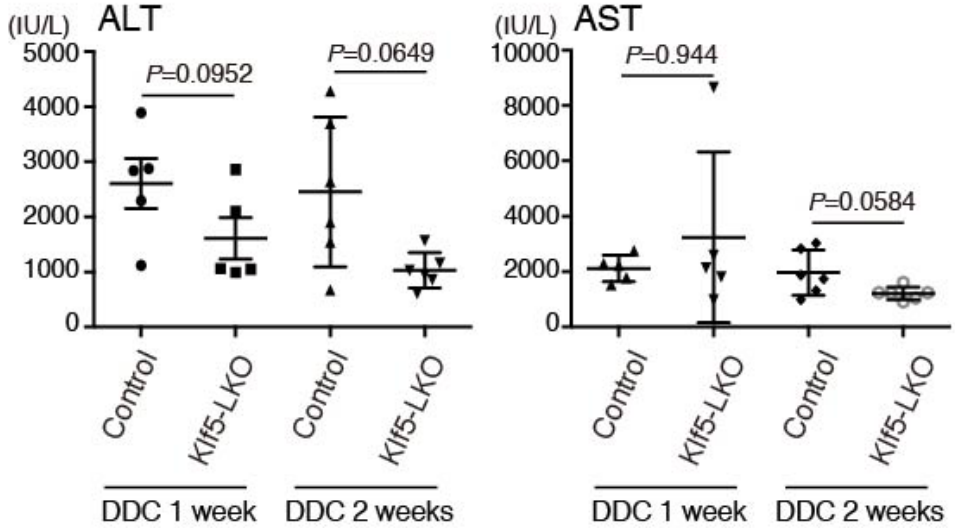
(IU/L)
ALT
5000
4000
3000
2000
1000
0
P=0.0952
P=0.0649
Control
Klf5-LKO
Control
Klf5-LKO
DDC 1 week
DDC 2 weeks
(IU/L)
AST
10000
8000
6000
4000
2000
0
P=0.944
P=0.0584
Control
Klf5-LKO
Control
Klf5-LKO
DDC 1 week
DDC 2 weeks

Figure 8. Survival curve and serum tests of Klf5 LKO mice upon DDC administration

(A) Kaplan–Meier survival curves of control (N = 49) and Klf5 LKO (N = 70) mice treated with DDC. (B) Serum T-BIL and ALP levels were measured in control and Klf5 LKO mice treated with DDC for one week (N = 5 mice) or two weeks (N = 6 mice). P-values calculated by Mann Whitney *U* test. (C) Serum ALT and AST levels in the Klf5 LKO and control mice upon DDC administration for one week (N = 5 mice for each group) or two weeks (N = 6 mice for each group), showing that hepatocyte injury was not exacerbated in the Klf5 LKO mice. P-values calculated by Mann Whitney *U* test.

A

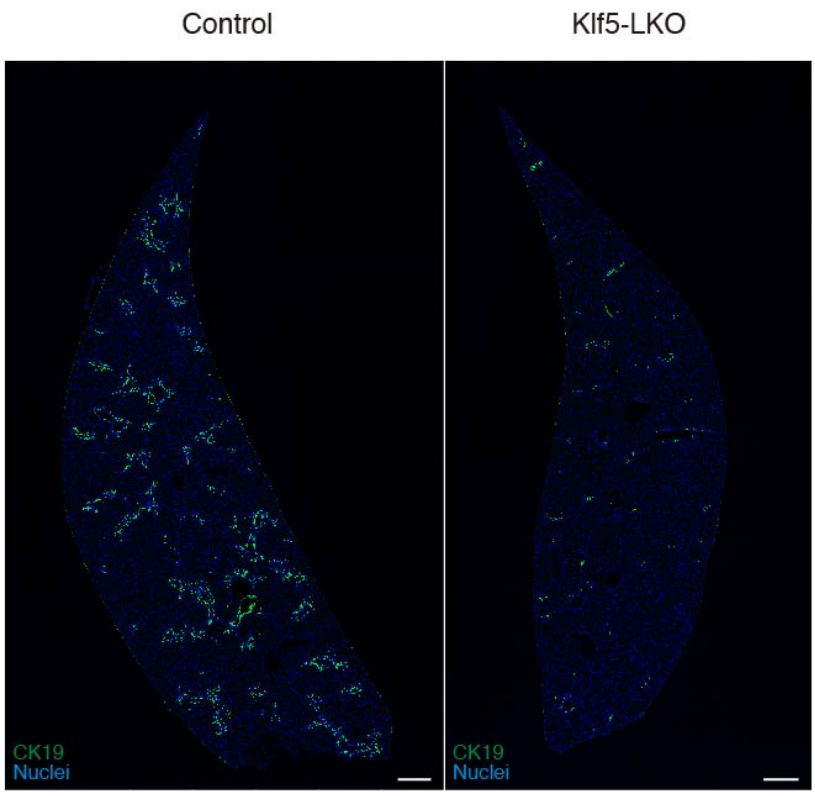
Control
Klf5-LKO
CK19
Nuclei
CK19
Nuclei

B

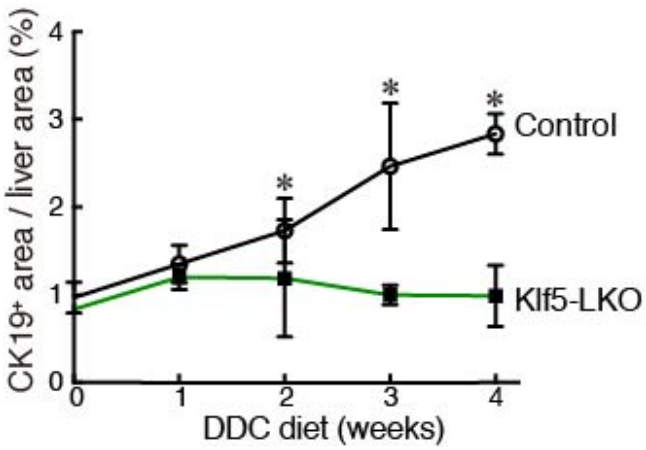
CK19+ area / liver area (%)
0
1
2
3
4
DDC diet (weeks)
Control
Klf5-LKO
*
*
*

Figure 9. DR induction upon DDC-induced liver injury is suppressed in Klf5 LKO mice.

(A) Representative images for CK19 immunostaining (green) of whole liver sections prepared form the control (left) and Klf5 LKO (right) mice treated with DDC for four weeks. Counterstaining for nuclei is also included (Blue). Scale bar = 500 μm. (B) Quantification of $CK19^+$ areas in whole liver sections. Data represent the mean ± SD. N ≥ 4 mice for each time points. P-values calculated by Mann Whitney *U* test for each time point comparing the control and Klf5 LKO mice and were as follows: 0.343 (DDC 0 week), 0.700 (DDC 1 week), 0.0207 (DDC 2 weeks), 0.0238 (DDC 3 weeks), and 0.0286 (DDC 4 weeks).

A

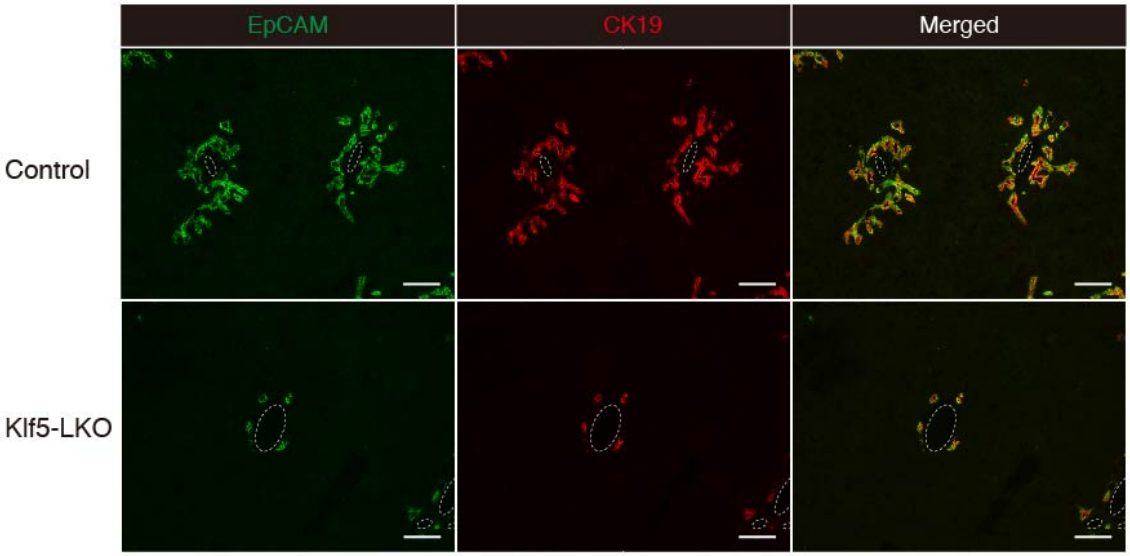

B

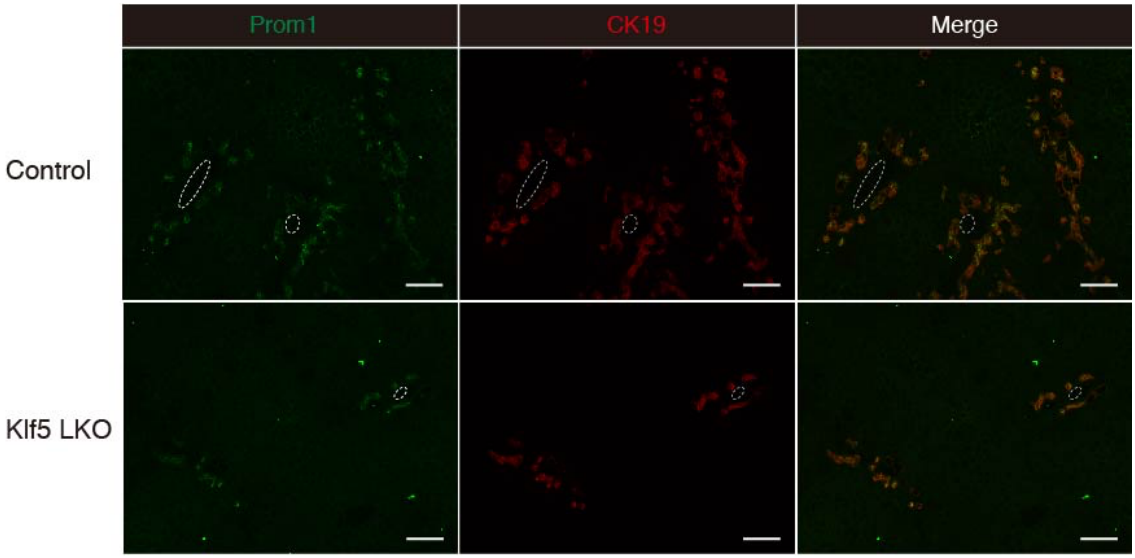

Figure 10. Immunostaining analyses employing other BEC markers

(A) Immunostaining for EpCAM (green) and CK19 (red) in the Klf5 LKO and control livers treated with DDC for four weeks. Scale bar = 100 μm. (B) Immunostaining for Prom1 (green) and CK19 (red) in the Klf5 LKO and control livers treated with DDC for four weeks. Scale bar = 100 μm.

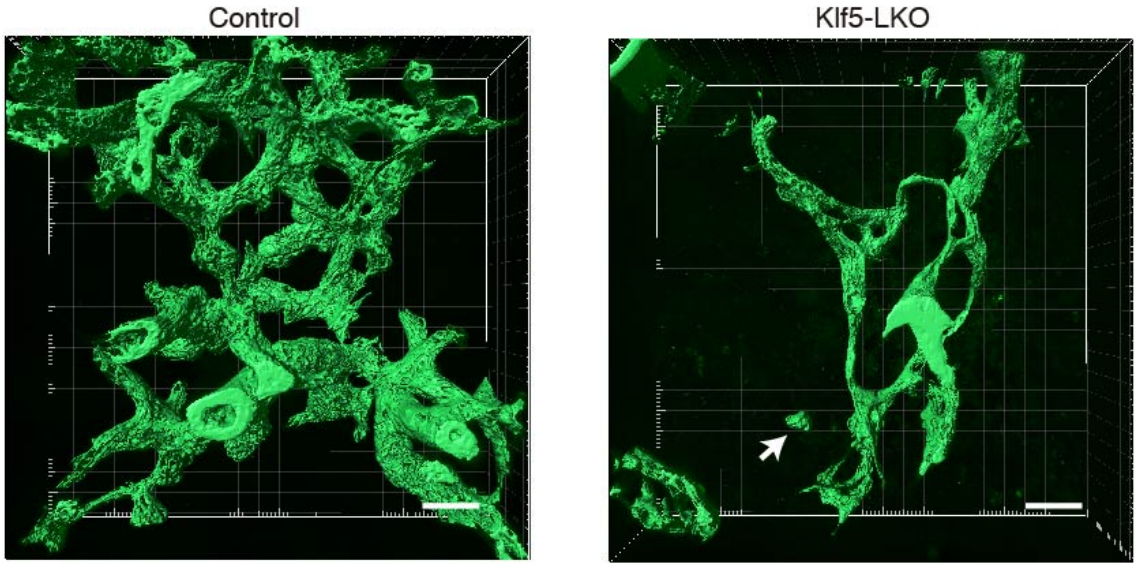

Figure 11. The biliary epithelial tissue morphology upon DDC adminstration at the three-dimensional (3D) level

3D immunostaining for CK19 (green) in the Klf5 LKO and control livers treated with DDC for 4 wk. Stacked images were obtained with confocal microscopy and used to reconstruct a 3D image using the IMARIS software. The image is shown in surface mode. Note that a $CK19^{+}$ cell cluster separated from the biliary tree structure is observed in the Klf5 LKO liver (white arrow). Scale bar = 50 μm.

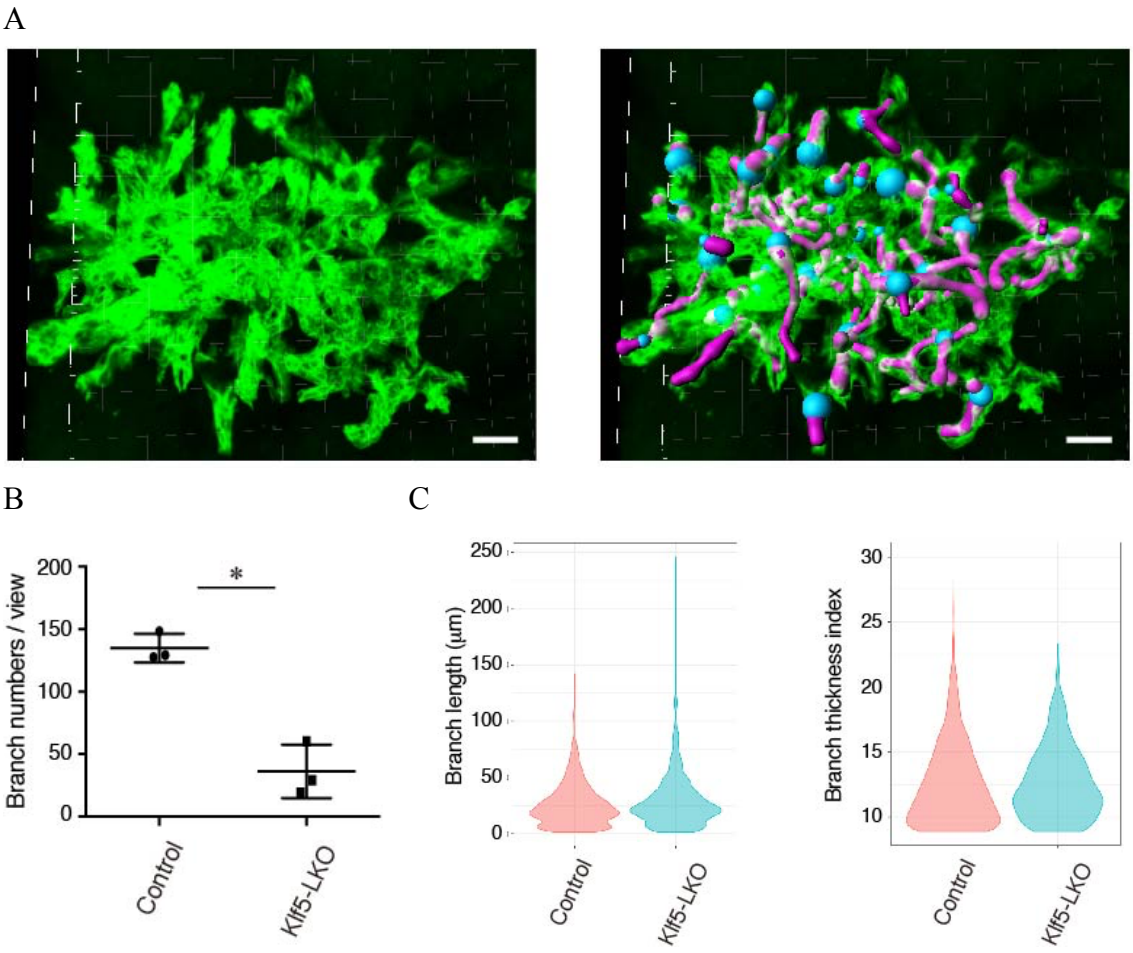

Figure 12. The biliary branch length and thickness quantification upon DDC administration

(A) Representative images for CK19 staining (green) and traced biliary branch structure (magenta in the right panel) for quantitative analyses of 3D immunostaining data. Scale bar = 50 μm. (B) The number of biliary branches per unit view field (636.396 μm × 636.396 μm × 200 μm) in the Klf5-LKO and control livers treated with DDC for four weeks. N = 3 mice for each group and more than 5 views were analyzed per mouse. P-value was calculated by Student *t* test to be 0.00540. (C) Violin plots comparing the length (left panel) and the thickness (right panel) of the biliary branches in the Klf5-LKO and control livers treated with DDC for four weeks. "Branch thickness index" was calculated as the square root of the quotient obtained by dividing the branch volume size by the branch length.

A

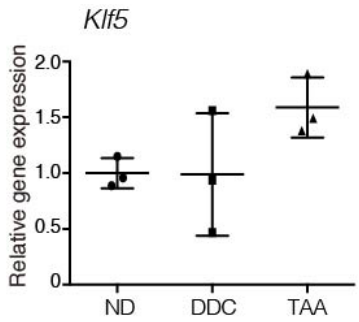
Klf5
Relative gene expression
2.0
1.5
1.0
0.5
0
ND
DDC
TAA

B

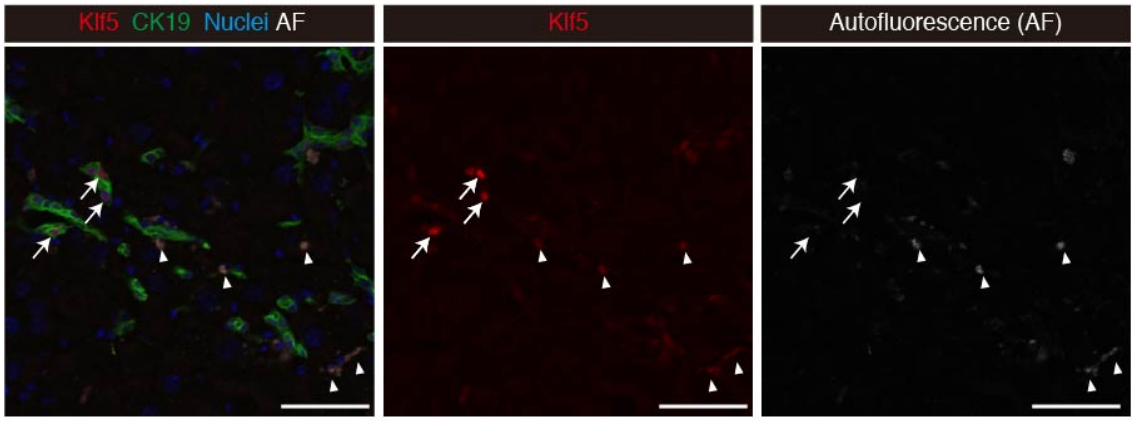
Klf5 CK19 Nuclei AF
Klf5
Autofluorescence (AF)

C

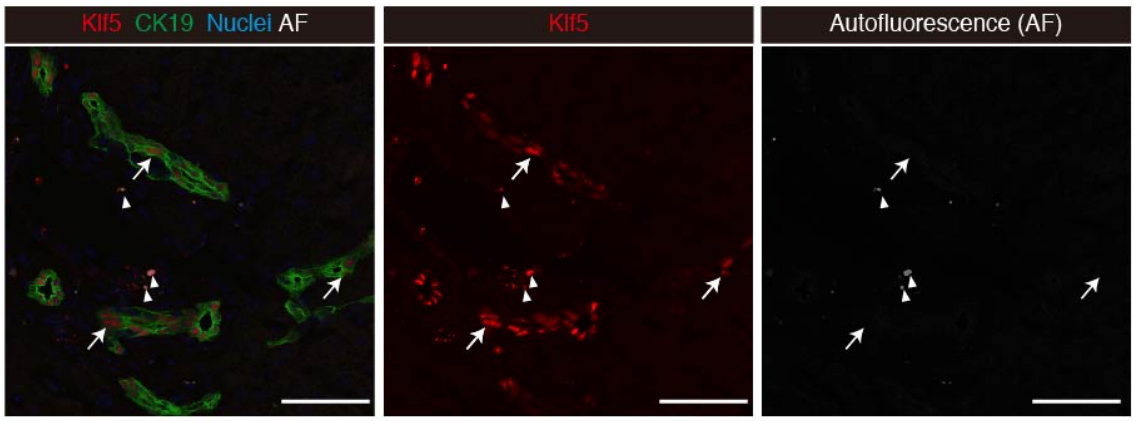
Klf5 CK19 Nuclei AF
Klf5
Autofluorescence (AF)

Figure 13. Klf5 expression patterns under liver injury conditions other than DDC liver injury.

(A) Expression levels of the *Klf5* in BECs under different injury conditions. mRNA samples were prepared from BEC fractions obtained from the WT mice under physiological conditions (fed normal diet: ND), upon DDC administration for five weeks, or upon TAA administration for eight weeks were subjected to quantitative RT-PCR analyses and subjected to quantitative RT-PCR analyses. P-value = 0.232 calculated by Kruskal-Wallis test. (B and C) Immunostaining for Klf5 (red) and CK19 (green) in the WT mouse liver upon TAA administration for eight weeks (B) and Abcb4 KO; $Klf5^{flox/flox}$ mouse (Abcb4 single knockout mouse) liver at eight weeks after birth (C). Counterstaining for nuclei is shown in blue. Non-specific autofluorescence signals (arrowheads) were acquired using a filter channel without any corresponding staining and are also shown in gray. Relevant signals for Klf5 are indicated by arrows. Scale bar = 50 mm.

A

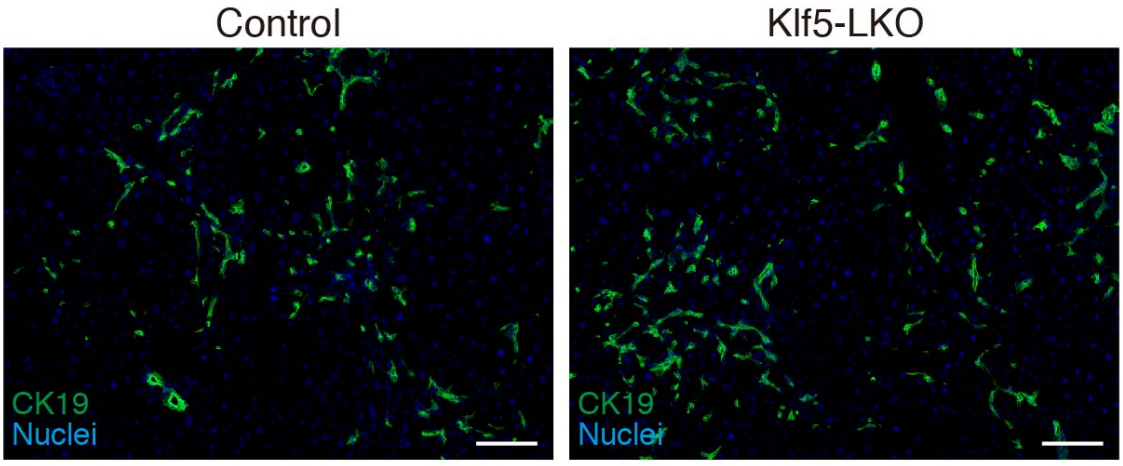

B

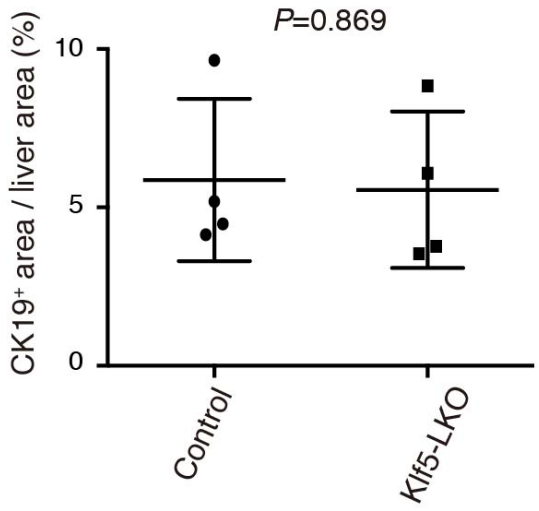

Figure 14. DR was not affected in Klf5 LKO mice upon TAA-injury

(A) Representative images of immunostaining for CK19 (green) in the Klf5 LKO and control livers treated with TAA for eight weeks. Counterstaining for nuclei is also included (Blue). Scale bar = 100 μm. (B) Quantification of $CK19^+$ areas in whole liver sections prepared from the TAA-treated mice as in (A). N = 4 mice for each group. P-values calculated by Student *t* test.

A

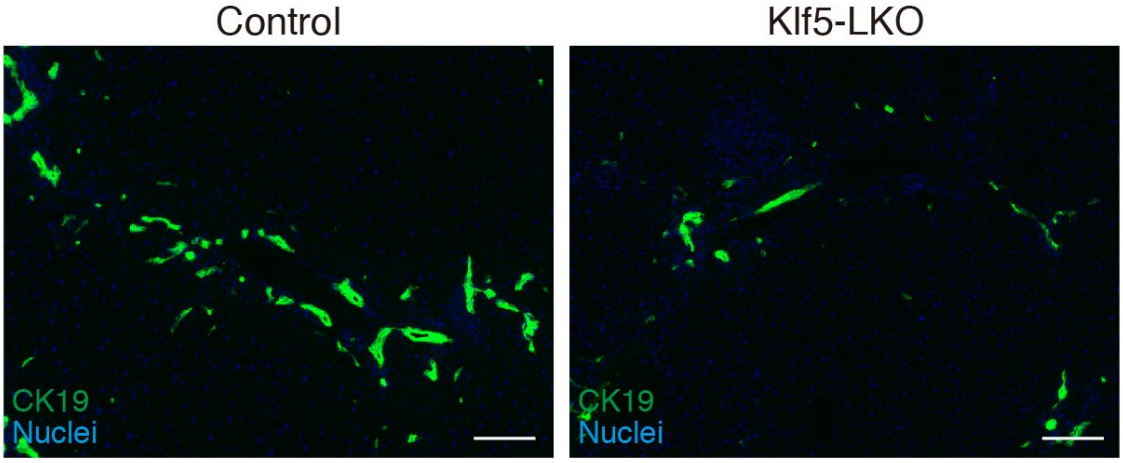

B

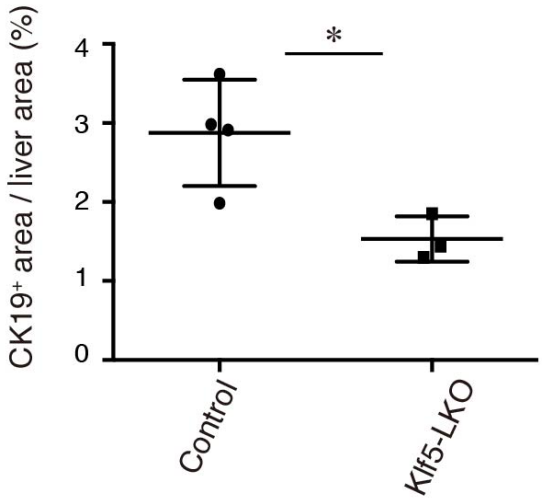

Figure 15. Loss of Klf5 affects DR induction specifically under cholestatic liver injury conditions.

(A) Representative images of immunostaining for CK19 (green) in the Abcb4 KO;Klf5 LKO double knockout and control (Abcb4 single knockout) livers at eight weeks after birth. Counterstaining for nuclei is also shown (Blue). Scale bar = 100 μm. (B) Quantification of $CK19^+$ areas in whole liver sections prepared from the Abcb4 KO cohorts as in (A). N = 4 and 3 mice for the control (Abcb4 single knockout) and the Klf5 LKO (Abcb4 KO; Klf5 LKO double knockout) groups, respectively. P-values calculated by Student *t* test.

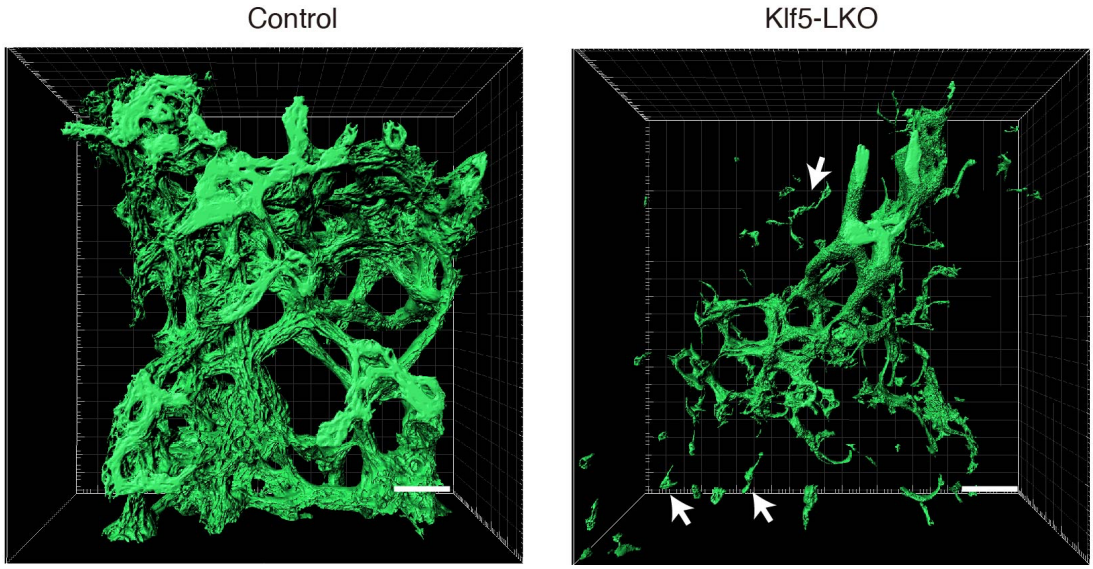

Figure 16 The biliary epithelial tissue morphology of the Abcb4 KO; Klf5 LKO double knockout mice at the three-dimensional (3D) level

3D immunostaining for CK19 (green) in the Abcb4 KO; Klf5 LKO double knockout and control (Abcb4 single knockout) livers at eight weeks after birth. Stacked images were obtained with confocal microscopy and used to reconstruct a 3D image using the IMARIS software. The image is shown in surface mode. White arrows indicate $CK19^{+}$ cells separated from the biliary tree structure. Scale bar = 50 μm.

A

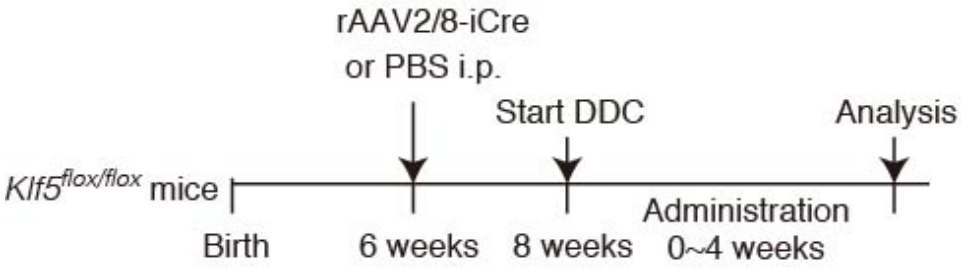

B

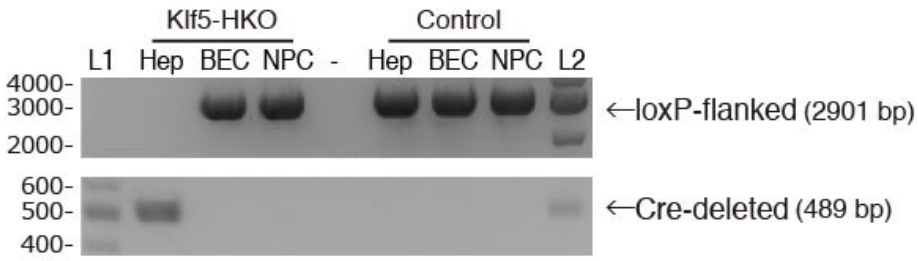

Figure 17. rAAV2/8-iCre mediated hepatocyte-specific deletion of *Klf5*

(A) Experimental scheme for analyses on the effect of hepatocyte-specific loss of Klf5. (B) Genomic PCR analysis for Cre-mediated recombination in the Klf5 locus. The upper and lower panels show amplicons corresponding to non-recombined (floxed) and recombined (Cre-deleted) alleles, respectively. The lanes indicated as L1 and L2 were loaded with 100 bp ladder and 1 kb ladder DNA size markers, respectively. The sizes of markers (bp) are indicated to the left.

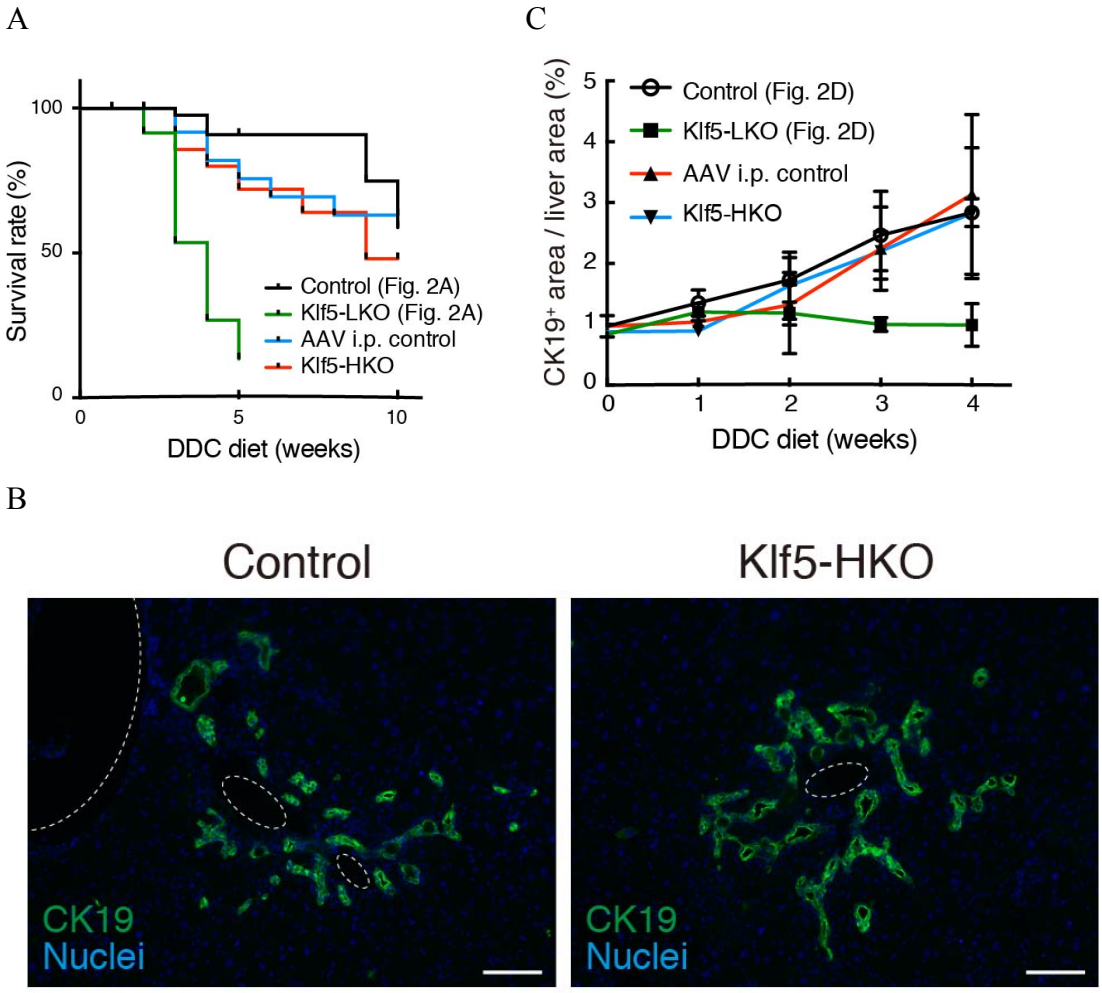

Figure18. Deletion of Klf5 in hepatocytes does not affect DR induction.

(A) Kaplan–Meier survival curves of control (N = 27) and Klf5 HKO (N = 30) mice treated with DDC. For comparison, the survival curves of Klf5-LKO and the control mice shown above in Figure 8A are also overlaid. (B) Immunostaining for CK19 (green) in the Klf5 LKO and control livers treated with DDC for four weeks shown with counterstaining for nuclei (Blue). Scale bar = 100 μm. (C) Quantification of $CK19^+$ areas in whole liver sections prepared from Klf5-HKO and AAV i.p. control mice. For comparison, the data of Klf5-LKO and the control mice shown above in Figure 9B are also overlaid. Data represent mean ± SD. N ≥ 3 mice for each time points. P-values calculated by Mann Whitney *U* test for each time points comparing the Klf5 HKO and control mice and were as follows: 0.100 (DDC 0 week), 0.100 (DDC 1 week), 0.400 (DDC 2 weeks), 0.900 (DDC 3 weeks), and 0.857 (DDC 4 weeks).

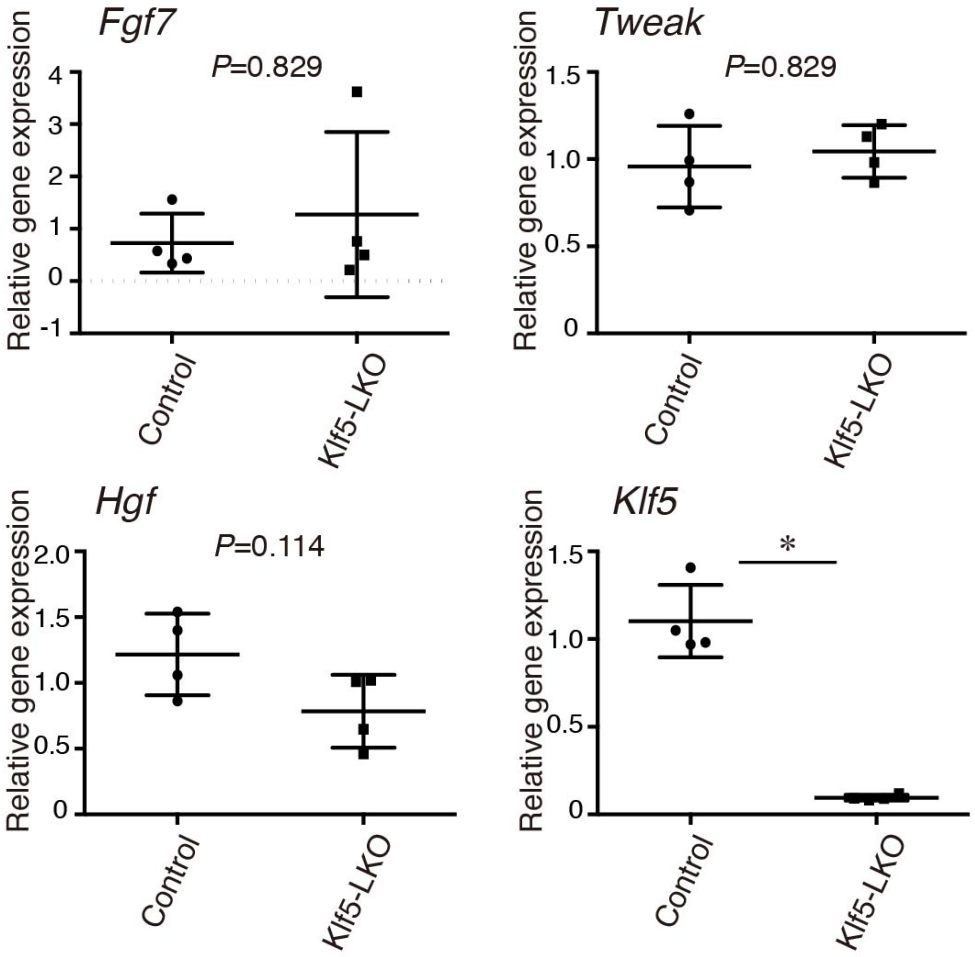

Figure 19. Expression levels of cytokines and growth factors involved in DR induction

Whole liver mRNA samples prepared from the control and Klf5 LKO mice treated with DDC for one week were subjected to quantitative RT-PCR analyses. N = 4 mice. P-values calculated by Mann Whitney *U* test.

GO Term	P-val
Mitotic nuclear division	3.80E-08
Cell division	1.76E-07
Cell cycle	1.51E-06
Mitotic spindle organization	1.65E-06
Regulation of cell cycle	3.05E-05

Figure 20. Transcriptome analysis by RNA-seq and subsequent DAVID gene ontology (GO) analysis

DEG were categorized in Biological GO terms using DAVID.

A

Downregulated GO gene sets	SIZE	NOM p-val	FDR q-val
GO_CELLULAR_COMPONENT_DISASSEMBLY	18	0	4.28E-02
GO_CHROMOSOME_SEGREGATION	21	0	6.61E-02
GO_SISTER_CHROMATID_SEGREGATION	18	1.39E-03	6.93E-02
GO_MITOTIC_CELL_CYCLE	48	0	7.10E-02
GO_NUCLEAR_CHROMOSOME_SEGREGATION	20	1.39E-03	7.41E-02
GO_CELL_DIVISION	35	0	9.16E-02
GO_REGULATION_OF_CHROMOSOME_SEGREGATION	8	0	9.43E-02
GO_CELL_CYCLE_PROCESS	57	1.17E-03	9.85E-02
GO_CELL_CYCLE	63	0	0.100
GO_EXTRACELLULAR_MATRIX_DISASSEMBLY	4	0	0.105
GO_ORGANELLE_FISSION	34	5.01E-03	0.113
GO_CYTOKINESIS	11	1.52E-03	0.119
GO_MITOTIC_NUCLEAR_DIVISION	30	0	0.137

B

Upregulated GO gene sets	SIZE	NOM p-val	FDR q-val
GO_OSSIFICATION	14	0.00E+00	1.01E-02
GO_G_PROTEIN_COUPLED_RECEPTOR_SIGNALING_PATHWAY	14	0.00E+00	1.18E-02
GO_REGULATION_OF_PHOSPHATIDYLINOSITOL_3_KINASE_SIGNALING	9	1.15E-02	0.204
GO_RESPONSE_TO_CYTOKINE	26	4.15E-03	0.214
GO_NEGATIVE_REGULATION_OF_CELL_PROLIFERATION	25	8.06E-03	0.228
GO_REGULATION_OF_MYELOID_LEUKOCYTE_DIFFERENTIATION	7	2.72E-03	0.231
GO_NEGATIVE_REGULATION_OF_VIRAL_PROCESS	5	2.46E-03	0.236
GO_CELLULAR_RESPONSE_TO_CYTOKINE_STIMULUS	21	0.00E+00	0.240
GO_REGULATION_OF_SMOOTHENED_SIGNALING_PATHWAY	4	2.43E-03	0.240
GO_NEGATIVE_REGULATION_OF_VIRAL_GENOME_REPLICATION	4	0.00E+00	0.248
GO_REGULATION_OF_MYELOID_CELL_DIFFERENTIATION	7	2.99E-03	0.249

C

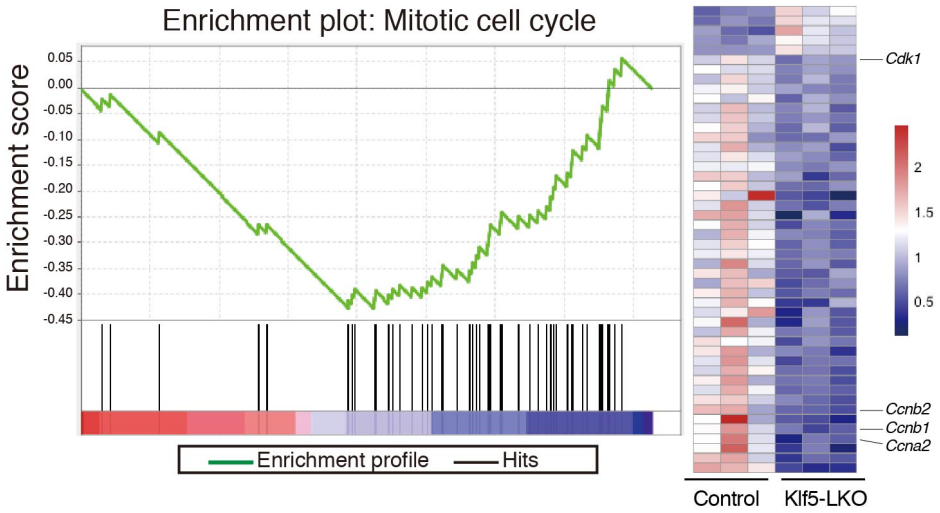

Figure 21. Transcriptome analysis by RNA-seq and subsequent Gene Set Enrichment Analysis (GSEA) reveals that Klf5 regulates cell proliferation in BECs.

(A and B) GSEA using DEG to identify enriched biological GO terms. The SIZE column indicates the number of genes hit in each gene set. The entire list of enriched gene sets categorized in GO biological process terms that were downregulated (A) and upregulated (B) by Klf5 deletion in BECs. Gene sets that meet the criteria for both NOM p-val < 0.05 and FDR q-val < 0.25 are considered to be significantly enriched and are listed. (C) A representative enrichment plot, corresponding to the "GO_MITOTIC_CELL_CYCLE" set in (A). The heat map shows expression levels of genes included in the gene set. The left three and right three columns correspond to BEC samples from the control and Klf5 LKO livers, respectively. The expression levels are indicated according to the scale bar to the right.

A

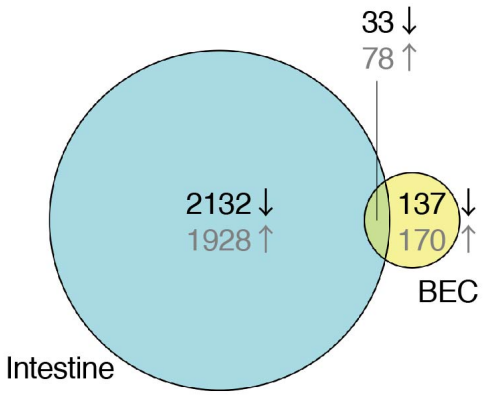

B

Common downregulated genes				
gene	baseMean	log2FoldChange	lfcSE	padj
Ccna2	567	-0.985	0.204	2.13E-04
Ccnb1	498	-0.948	0.189	9.62E-05
Cdk1	768	-0.492	0.165	0.089
Downregulated genes only in the intestine				
gene	baseMean	log2FoldChange	lfcSE	padj
Ccnd1	2525	0.042	0.152	0.969
Ccne1	170	-0.431	0.211	0.413
Downregulated genes only in BEC				
gene	baseMean	log2FoldChange	lfcSE	padj
Ccnb2	598	-0.947	0.189	9.62E-05

C

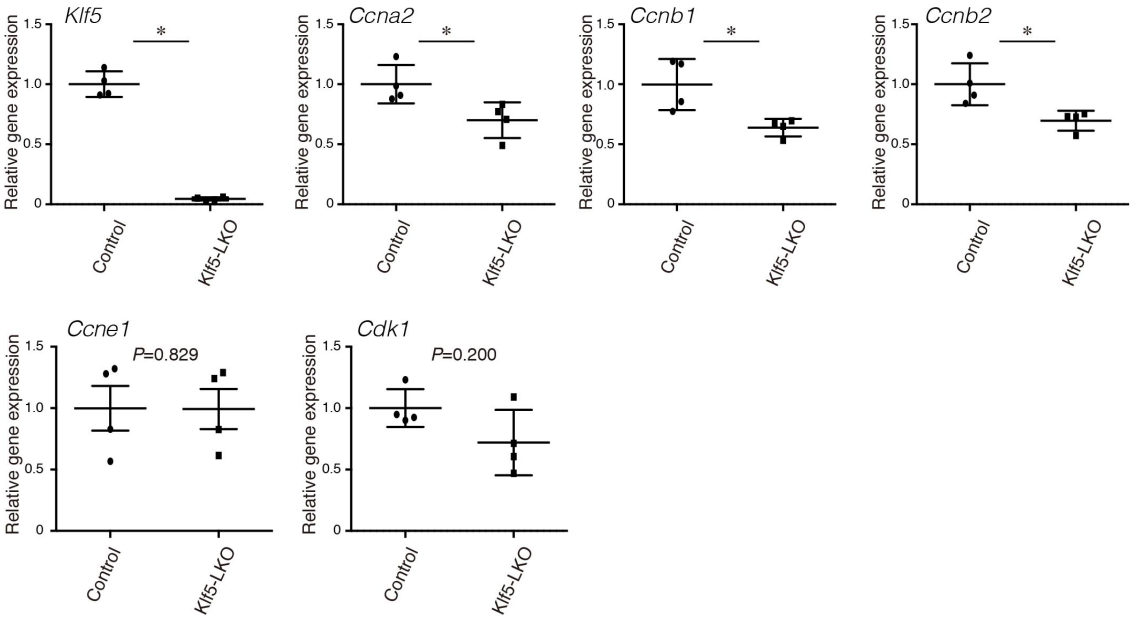

Figure 22. The cell cycle related genes affected in BECs not necessarily consistent with those in the intestine

(A) Venn diagram showing DEG identified in the intestine (left circle) and BECs (right circle) upon Klf5 deletion. Numbers shown in black and gray characters in the diagram indicate the counts of downregulated and upregulated genes, respectively. (B) RNA-seq data for expression levels for cell cycle-related genes. Three categories correspond to those in the Venn diagram shown in (A). (C) Expression levels of cell cycle-related genes. BECs mRNA samples prepared from the control and Klf5 LKO mice treated with DDC for two weeks were subjected to quantitative RT-PCR analyses. N = 4 mice. P-values were calculated by Mann Whitney *U* test and were as follows: 0.0286 (*Klf5*), 0.0286 (*Ccna2*), 0.0286 (*Ccnb1*), and 0.0286 (*Ccnb2*).

A

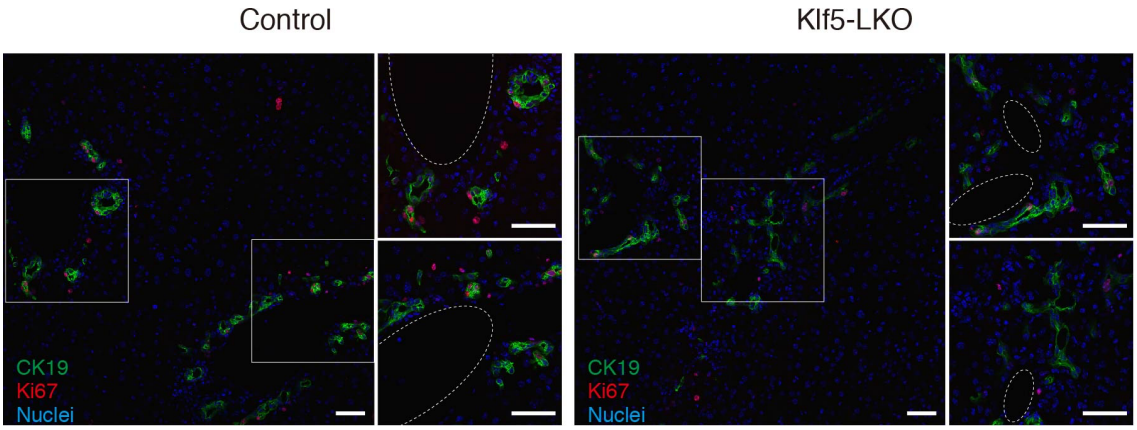

B

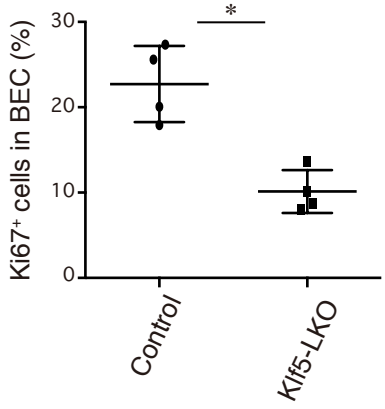

Figure 23. Immunostaining liver sections of Klf5 LKO mice upon DDC administration for the proliferation marker Ki67

(A) Immunostaining for Ki67 (red) and CK19 (green) in the Klf5 LKO and control livers treated with DDC for one week shown with counterstaining for nuclei (Blue). Two regions of interest indicated by white boxes in the left panels are magnified in the right panels. Scale bar = 50 μm. (B) Quantification of $Ki67^+$ cells in the $CK19^+$ BEC population. N = 4 mice. P-values calculated by Student *t* test.

A

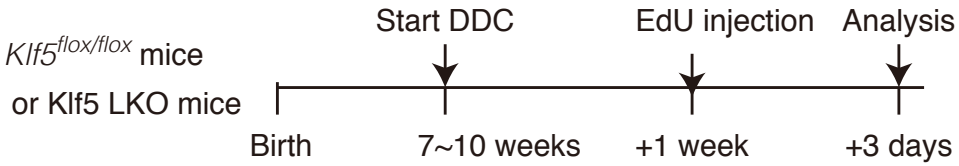

B

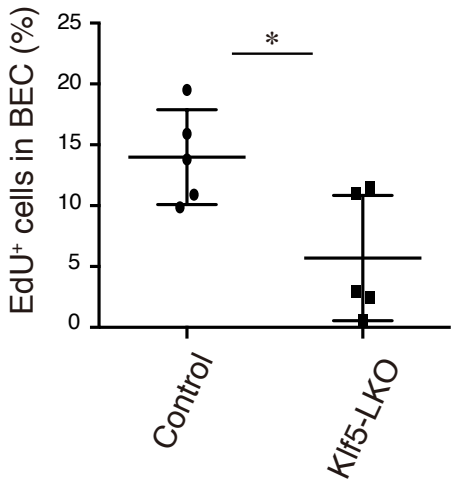

Figure 24. EdU incorporation by BECs in Klf5 LKO mice upon DDC administration

(A) Experimental scheme of EdU incorporation experiment in Klf5 LKO mice. (B) Quantification of EdU^+ cells in BECs as revealed by flow cytometry analyses. N = 5 mice. P-value was calculated by Student *t* test to be 0.0224.

A

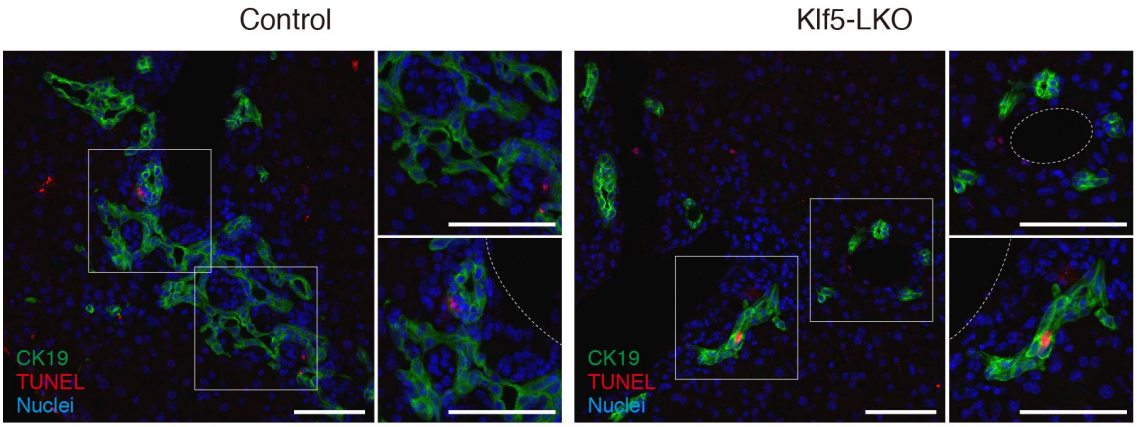

B

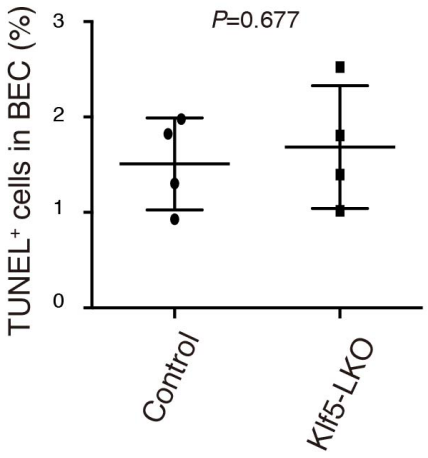

Figure 25. Detecting dead cells in liver sections of Klf5 LKO mice upon DDC administration

(A) TUNEL staining (red) was performed to detect apoptotic cells with co-immunostaining for CK19 (green) in the Klf5 LKO and control livers treated with DDC for two weeks. Counterstaining for nuclei is also shown (Blue). Scale bar = 50 μm. (B) Quantification of $TUNEL^+$ cells in the $CK19^+$ BEC population. N = 4 mice. P-values calculated by Student *t* test.

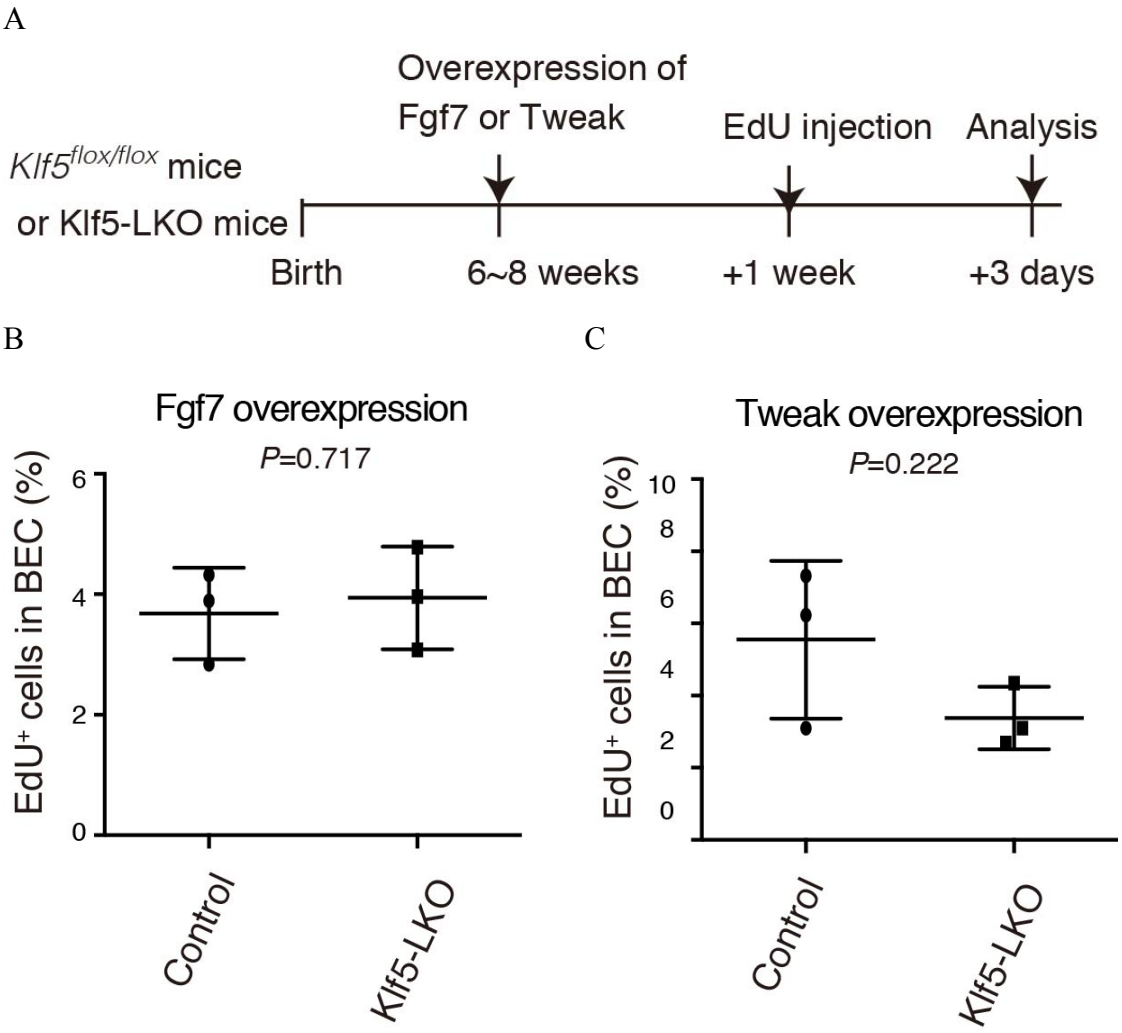

Figure 26. Fgf7 and Tweak affect BECs proliferation independent of Klf5

(A) Experimental scheme of EdU incorporation experiment in Klf5 LKO mice in which livers Fgf7 or Tweak were overexpressed by hydrodynamic delivery of the expression plasmid. (B) Quantification of EdU-positive BECs from Fgf7 overexpressed livers of the control and Klf5 LKO mice by flow cytometry in cells isolated from mice. N = 3 mice. P-values calculated by Student *t* test. (C) Quantification of EdU-positive BECs from Tweak overexpressed livers of the control and Klf5 LKO mice by flow cytometry in cells isolated from mice. N = 3 mice. P-values calculated by Student *t* test.

A

Downregulated KEGG pathway gene sets	SIZE	NOM p-val	FDR q-val
KEGG_SMALL_CELL_LUNG_CANCER	7	2.50E-02	0.137
KEGG_GLUTATHIONE_METABOLISM	6	1.44E-02	0.167
KEGG_FOCAL_ADHESION	11	4.22E-02	0.186
KEGG_ECM_RECEPTOR_INTERACTION	6	1.58E-02	0.190

B

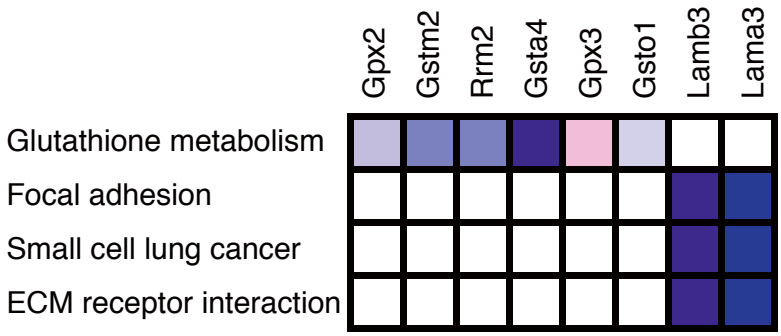

Figure 27. GSEA pathway analysis and leading edge analysis

(A) The entire list of enriched KEGG pathway gene sets. The SIZE column indicates the number of genes hit in each gene set. Gene sets that meet the criteria for both NOM p-val < 0.05 and FDR q-val < 0.25 are considered to be significantly enriched and are listed. (B) Leading edge analysis of the entire list of enriched KEGG pathway gene sets shown in (A). The range of colors in the heatmap (pink, light blue, and dark blue) corresponds to the range of gene expression values (moderate, low, and lowest, respectively).

A

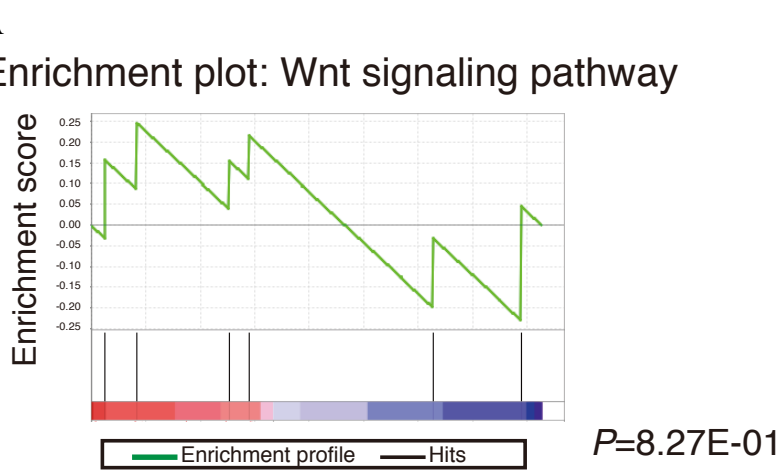

B

gene	baseMean	log2FC	lfcSE	padj
Notch1	193	-0.001	0.214	0.999
Notch2	700	0.091	0.167	0.925
Hes1	14419	0.158	0.210	0.890
Hey1	23	0.201	0.172	0.770
Jag1	14211	0.145	0.151	0.836

Figure 28. Neither Notch or Wnt signaling was significantly affected in the absence of Klf5 expression

(A) Wnt signaling pathway enrichment plot. NOM p-val = 0.817 and FDR q-val = 0.950. (B) Expression levels of Notch signaling-related genes as revealed by RNA-seq analysis.

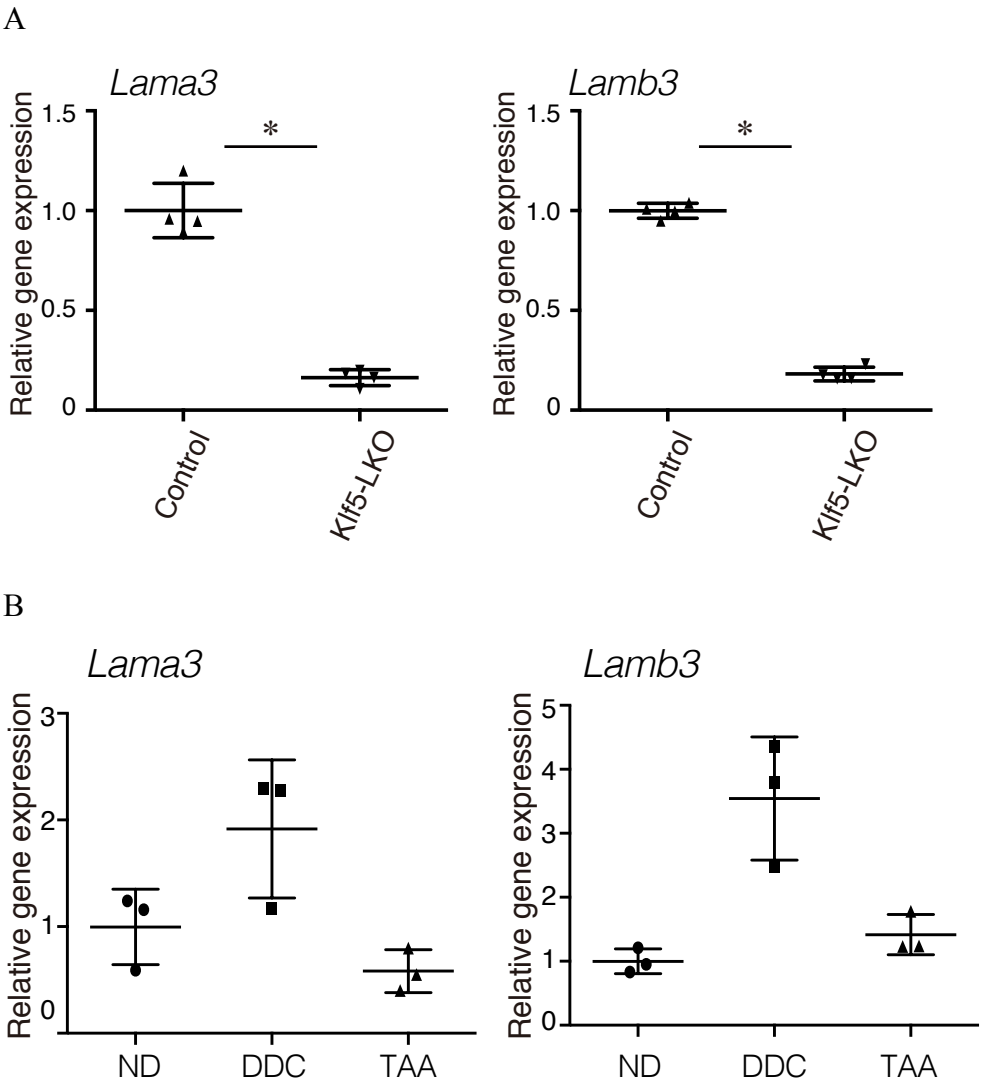

Figure 29. Candidate downstream molecules of Klf5

(A) Expression levels of the *Lama3* and *Lamb3*. BECs mRNA samples prepared from the control and Klf5 LKO mice treated with DDC for two weeks were subjected to quantitative RT-PCR analyses. N = 4 mice. P-values were calculated by Mann Whitney *U* test and were as follows: 0.0286 (*Lama3*) and 0.0286 (*Lamb3*). (B) Expression profiles of *Lama3* and *Lamb3* in BECs upon liver injury. BEC mRNA samples prepared from the WT mice under physiological conditions (fed normal diet: ND), upon DDC administration for five weeks, or upon TAA administration for eight weeks were subjected to quantitative RT-PCR analyses. P-values were calculated by Kruskal-Wallis test and were as follows: 0.0286 (*Lama3*) and 0.00360(*Lamb3*).

A

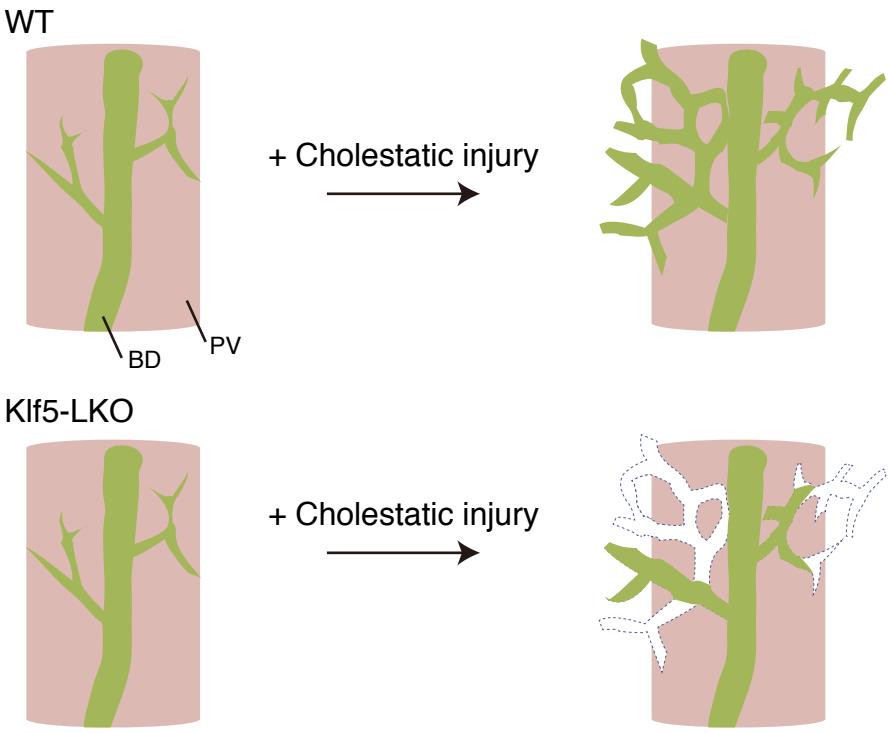

B

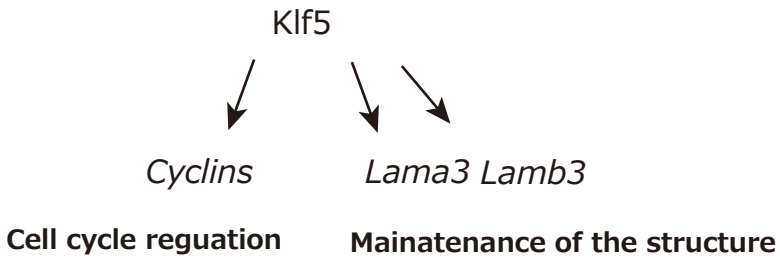

Figure 30. Klf5 plausible DR regulation mechanism

(A) Model of biliary remodeling under the cholestatic liver-injury. Upper diagrams show the normal remodeling and lower diagrams show the remodeling defect due to the loss of Klf5. Abbreviations: BD, bile duct; PV, portal vein. (B) Scheme of Klf5 downstream targets and functions under the cholestatic liver-injury.

Table 1. List of primers used for quantitative RT-PCR in this study

Gene	Direction	Sequence (5' to 3')
Ccna2	Forward	CTTGGCTGCACCAACAGTAA
	Reverse	CAAACTCAGTTCTCCCAAAAACA
Ccnb1	Forward	ACCAGAGGTGGAACTTGCTG
	Reverse	GGCTTGGAGAGGGATTATCA
Ccnb2	Forward	TGAAACCAGTGCAGATGGAG
	Reverse	CAGAGAAAGCTTGGCAGAGG
Ccne1	Forward	TTGCAAGACCCAGATGAAGA
	Reverse	TCCACGCATGCTGAATTATC
Cdk1	Forward	TCCGTCGTAACCTGTTGAGT
	Reverse	TGGCCAGTGACTCTGTGTCT
Epcam	Forward	AGGGGCGATCCAGAACAACG
	Reverse	ATGGTCGTAGGGGCTTTCTC
Fgf7	Forward	TTTGGAAAGAGCGACGACTT
	Reverse	GGCAGGATCCGTGTCAGTAT
Gapdh	Forward	TGTGTCCGTCGTGGATCTGA
	Reverse	TTGCTGTTGAAGTCGCAGGAG
Hgf	Forward	CCCGAGAACTTCAAATGCAA
	Reverse	TATGACGGTGTAAATCCTCCA
Klf5	Forward	TGCGATTATAATGGTTGCACA
	Reverse	GGTGCACTTGTAGGGCTTCT
Lama3	Forward	TGTACCTTGGGAATAAGGATGC
	Reverse	CGTCAGGACCTGGTCTATCTG
Lamb3	Forward	AGCCAGCAGGCAATGAAT
	Reverse	GCCGGTCCTTCAACTCTGTAT
Tat	Forward	CATCTGGAGCCATGTACCTT
	Reverse	TCCAGCATCATCACCTCG
Tweak (Tnfsf12)	Forward	GCCCATTATGAGGTTCATCC
	Reverse	TCACTGTCCCATCCACACC

Table 2. List of primers used for genomic PCR in this study

Gene	Direction	Sequence (5' to 3')
Klf5	Forward	GTAATGGATGTGAACAGATTTGAGG
	Reverse	GTAAACACTGCCGTTTACGTTTTGA

Table 3. List of antibodies used in this study

Antigen	Source / Supplier	Host	Fixation	Dilution	Ref.
CD45*	BD Pharmingen (Franklin Lakes, NJ), Cat. No. 553081	Rat	No fixation	1/100	
CK19	In-house	Rabbit	PFA only or Acetone & PFA	1/2000	(66)
EpCAM	BD Pharmingen (Franklin Lakes, NJ), Cat. No. 552370	Rat	Acetone & PFA	1/200	
EpCAM*	In-house	Rat	No fixation	1/100	(26)
Ki67	invitrogen (Carlsbad, CA), Cat. No. 14-5698-82	Rabbit	PFA	1/200	
Klf5	Generous gift from Drs. Ryozo Nagai (Jichi Medical University, Tochigi, Japan) and Ichiro Manabe (Chiba University, Chiba, Japan) (KM1784)	Rat	PFA	1/300	(67)
Prominin1	Biolegend (San Diego, CA), Cat. No. 141207	Rat	Acetone	1/100	

*These antibody were used for FACS. The others were used for immunostaining.

Acknowledgments

The present study was performed under the supervision of Professor A. Miyajima and Associate professor T. Itoh. I would like to express my great appreciation to their mentorship and support. I thank gratefully Dr. Kaneko and Dr. Kamimoto for their technical instructions and exciting and helpful discussion. I sincerely thank M. Yamada for the technical instructions, the recombinant AAV, and helpful discussion.

I thank gratefully Masatsugu Ema (Shiga University of Medical Science, Shiga, Japan) for collaborations with my research and *Klf5* flox mice.

I thank Dr. C. Y. Kok for the recombinant AAV, Dr. L. W. Katsumata for technical instructions, N. Miyata and C. Koga for cell sorting, N. Imaizumi for animal care, and the members of the Miyajima lab for helpful discussions and advice. I thank Prof. Ryozo Nagai (Jichi Medical University, Tochigi, Japan) and Prof. Ichiro Manabe (Chiba University, Chiba, Japan) for the anti-Klf5 antibody; Prof. Klaus Kaestner (University of Pennsylvania, USA) for the Alfp-Cre Tg mouse; Prof. Ian Alexander (Children's Medical Research Institute, Australia) for the pAM-LSP1-EGFP plasmid; Prof. R Jude Samulski and the NGVB Biorepository (University of North Carolina at Chapel Hill, USA) for the XX6-80 plasmid; Prof. Rolf Zeller for the pDIRE plasmid; and Penn Vector Core (University of Pennsylvania, USA) for the p5E18-VD2/8 plasmid; Prof. Yuki Kato and Katsuhiko Shirahige (Insutitute of Molecular and Cellular Biosciences, the University of Tokyo, Japan) for RNA-sequecning. I also thank The University of Tokyo IMCB Olympus Bioimaging Center (TOBIC) for helping with microscopy and image acquisition.